



Radiolabeling of Theranostic Nanosystems

Sudeep Das, Surachet Imlimthan, Anu J. Airaksinen,
and Mirkka Sarparanta

Abstract

In the recent years, progress in nanotechnology has significantly contributed to the development of novel pharmaceutical formulations to overcome the drawbacks of conventional treatments and improve the therapeutic outcome in many diseases, especially cancer. Nanoparticle vectors have demonstrated the potential to concomitantly deliver diagnostic and therapeutic payloads to diseased tissue. Due to their special physical and chemical properties, the characteristics and function of nanoparticles are tunable based on biological molecular targets and specific desired features (e.g., surface chemistry and diagnostic radioisotope labeling). Within the past decade, several theranostic nanoparticles have been developed as a multifunctional nanosystems which combine the diagnostic and therapeutic functionalities into a single drug delivery platform. Theranostic nanosystems can provide useful information on a real-time systemic distribution of the developed nanosystem and simultaneously transport the therapeutic payload. In general, the diagnostic functionality of theranostic nanoparticles can be achieved through labeling gamma-emitted radioactive isotopes on the surface of nanoparticles which facilitates noninvasive detection using nuclear molecular imaging techniques, such as positron emission tomography (PET) and single-photon emission computed tomography (SPECT), meanwhile, the therapeutic effect arises from the potent drug released from the nanoparticle. Moreover, some radioisotopes can

concurrently emit both gamma radiation and high-energy particles (e.g., alpha, beta, and Auger electrons), prompting the use either alone for radiotheranostics or synergistically with chemotherapy. This chapter provides an overview of the fundamentals of radiochemistry and relevant radiolabeling strategies for theranostic nanosystem development as well as the methods for the preclinical evaluation of radiolabeled nanoparticles. Furthermore, preclinical case studies of recently developed theranostic nanosystems will be highlighted.

Keywords

Radiochemistry · Radiolabeling · Nuclear imaging
Molecular imaging · Theranostic nanosystem
Nanotheranostic

1 Introduction

The term *theranostic* coined by the merging of the terms “therapeutic” and “diagnostic,” refers to multifunctional nanosystems that are able to provide both therapeutic (e.g., delivery of a chemotherapeutic payload) and diagnostic (e.g., imaging or therapy monitoring) functions in the same platform. Radioisotopes can be employed in two ways for the development of theranostic nanosystems. First, the nanosystems can be radiolabeled with imaging-compliant isotopes such as those utilized for positron emission tomography (PET) or single-photon emission computed tomography (SPECT), which emit gamma radiation that can be detected and quantified noninvasively outside of the subject using dedicated imaging systems [1]. This will give information on the localization of the nanosystem in the body, including the targeting ability, kinetics of nanomaterial tumor accumulation, the route and rate of nanosystem elimination, and the circulation time. This information provides vital feedback on

S. Das · S. Imlimthan · M. Sarparanta (✉)
Department of Chemistry, University of Helsinki,
Helsinki, Finland
e-mail: mirkka.sarparanta@helsinki.fi

A. J. Airaksinen
Department of Chemistry, University of Helsinki,
Helsinki, Finland

Turku PET Centre, Department of Chemistry, University of Turku,
Turku, Finland

the performance of the nanosystem based on its structure–activity relationship, and guides future structural optimization for improved in vivo behavior. Additionally, when radiolabeled with diagnostic radioisotopes, the nanosystems can be used to screen for patients who will have sufficiently high nanosystem tumor accumulation to permit the attainment of therapeutically relevant payload concentrations in the tumor. In this way, the nanosystem itself can be used for patient stratification instead of a surrogate imaging biomarker. Second, the highly energetic particle radiation (α , β^- , and Auger electrons), arising from radioactive decay of radioisotopes conjugated to the nanosystem, can be employed as a therapeutic strategy either alone or synergistically with chemotherapy [2]. Due to their high molar activity, therapeutic radioisotopes are lucrative payloads for theranostic nanosystem development, as very small amounts of the radioisotope are often enough to impart therapeutically relevant radioactive doses at the tumor. This is in contrast to the feasibility limitations set by a limited drug loading degree in many cancer-targeting nanosystems under development today.

In this chapter, we will give an overview of the current and emerging radiolabeling strategies for the radiolabeling of theranostic nanosystems either for imaging, radiotherapy, or combination of the two, as well as provide a basic outline for the biological evaluation of radiolabeled theranostic nanosystems. Finally, a review of selected contemporary examples of preclinical and clinical studies utilizing radiolabeled theranostic nanosystems is given.

2 Key Concepts in Radiochemistry for Theranostic Nanosystem Development

2.1 Radioactive Decay and Properties of Radiolabeled Tracers

Radioactive decay results when a nucleus has too much mass or an improper proton-to-neutron ratio to remain stable: the nucleus becomes unstable and either emits a bulky particle to reduce its mass (α decay) or transfers one proton to a neutron or neutron to a proton to balance the proton-to-neutron ratio (β^+ or electron capture decay or β^- decay). In α decay, an energetic α particle (a nucleus of a helium atom) is emitted, whereas in a beta decay the outgoing particles are either β^+ (positron) or β^- (electron). In addition to these decays a number of different types of electromagnetic (gamma radiation, X-rays) and electron (conversion and Auger electrons) radiation is emitted while the nuclei formed in excited state in the decay event will de-excite. All these modes of radiation are collectively known as *ionizing radiation*. A stable nucleus can be attained either by a single decay of an unstable nucleus

(as for the isotope fluorine-18 (^{18}F in Fig. 1a) or as a result of a decay chain, where the energy is lost in a series of decays through different daughter nuclei like in the case of the alpha emitter actinium-225 (^{225}Ac , Fig. 1b).

The fundamental premise to the use of radiolabeled compounds as *tracers* for the respective nonradiolabeled compounds is that radioactive isotopes behave chemically identically to the nonradioactive isotopes of the same element. The terms *tracer*, *imaging probe*, and *imaging agent* are used interchangeably in the literature and all refer to radiolabeled compounds used to track a structurally identical nonradiolabeled compound in vivo.

The most important properties of a radioisotope from the theranostic standpoint are the quality and energy of the emitted radiation, the physical half-life ($t_{1/2}$) of the radioisotope, and the chemical characteristics of the element in question. Highly tissue-penetrant gamma radiation is needed for non-invasive nuclear imaging, whereas particle radiation is needed for the deposition of energy into the tumor tissue through the interactions between the tissue and the emitted charged particles. The amount of energy deposited in tissue is determined by the linear energy transfer (LET) value, and it is determined by the path length of the particle in the tissue and the energy of the radiation. Out of the charged particles, helium nuclei (α particles) and Auger electrons have the highest LET values with the path length tens of micrometers (α particles) or mere fractions of a micrometer (Auger electrons), while higher-energy electrons (β particles and conversion electrons) travel millimeters depending on their energy, and consequently have lower LET values as illustrated with an example of radioimmunoconjugates in Fig. 2. The range of the particle radiation in tissue should be matched to the dimensions of the tumor to ensure homogenous deposition of the energy in the tumor tissue as illustrated in Fig. 3.

The radionuclide half-life is determined by Eq. 1,

$$t_{1/2} = \frac{\ln 2}{\lambda} \quad (1)$$

where λ is the decay constant for the radioisotope. The half-life tells us the amount of time required for the radioactivity (A) of the material to decrease to one half of the original value (A_0) and can be used to calculate the amount of radioactivity remaining in a sample at a given time t as shown in Eq. 2.

$$A = A_0 e^{-\lambda t} = A_0 \times 2^{-t/t_{1/2}} \quad (2)$$

The physical half-lives of radioactive isotopes vary from fractions of a second to billions of years. For isotopes relevant for the development and radiolabeling of theranostic nanosystems, the half-lives are most typically in the order of hours to several days. This has a number of practical implications to the nanosystem development and choice of the radio-

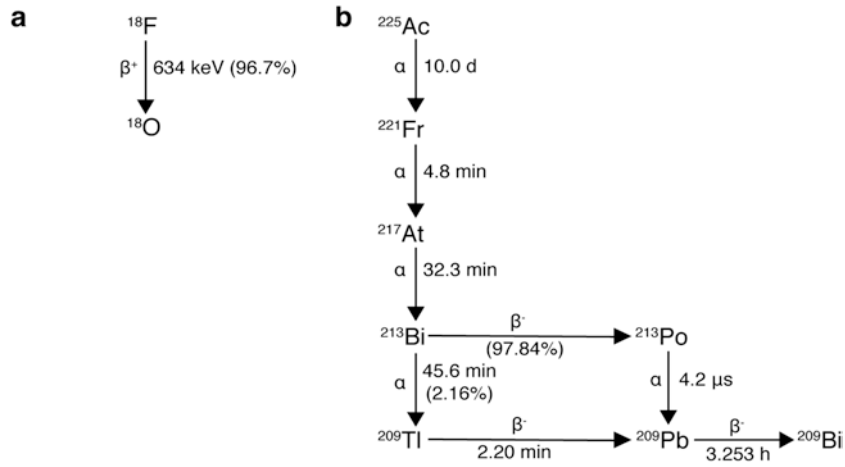


Fig. 1 Radioactive decay can occur with a single emission or by multiple decays referred to as a “decay chain”. The short-lived positron emitter ^{18}F (a) decays predominantly by positron emission

(the rest is by electron capture), whereas heavy ^{225}Ac (b) decays by a series of alpha and beta decays through a number of daughter nuclei

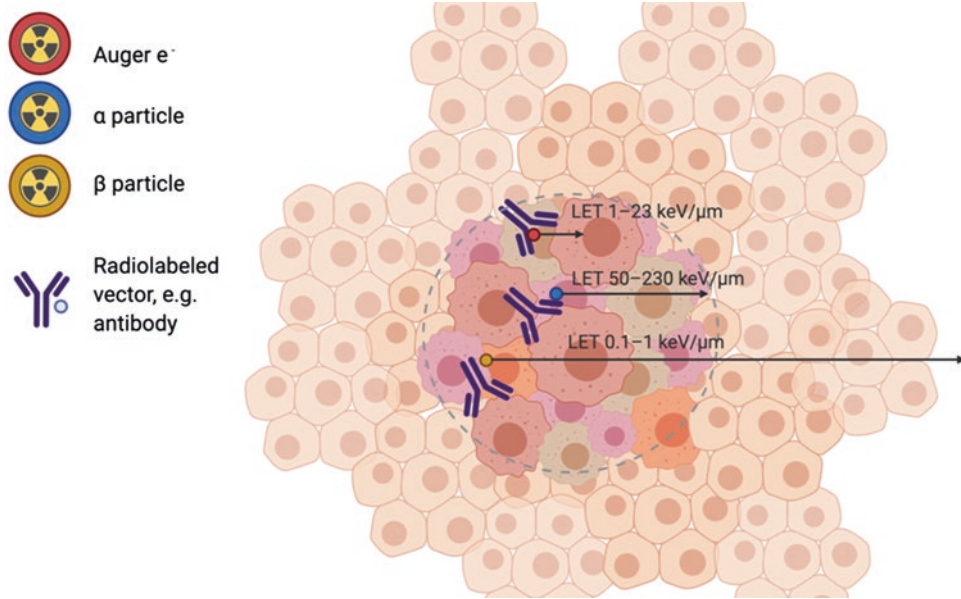


Fig. 2 Illustration of the track of α -particles, β -particles, and Auger electrons emitted by radiolabeled monoclonal antibodies targeted to cancer cells. The short track length of α -particles (28–100 μm) and Auger electrons (<0.5 μm) results in high linear energy transfer (LET) values of 50–230 keV/ μm and 1–23 keV/ μm , respectively. β -Particles

have a track length of 2–10 mm in tissue resulting in LET of 0.1–1.0 keV/ μm . The high LET of α -particles and Auger electrons makes these forms of radiation more powerful for killing cancer cells than β -particles. (Figure adapted from references [3, 4])

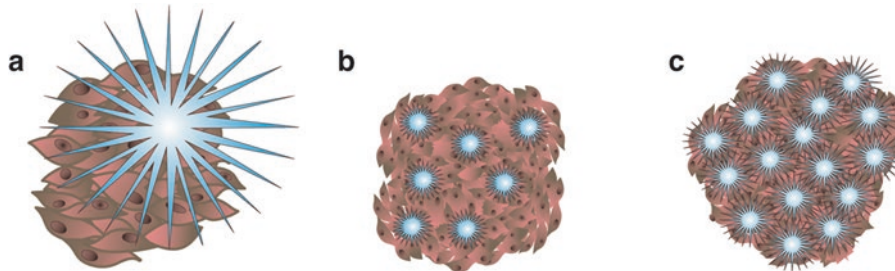


Fig. 3 Matching the range of the radioactive emission to the dimensions of the target is important for the efficacy of the radiotherapy. Subpar effects will be seen in a small tumor treated with long-range (low LET) irradiation (a) or in a large mass treated with a short-range

(high LET) irradiation with heterogenous distribution (b), whereas optimal results are achieved when a relatively homogenous distribution of an intermediate LET radioisotope is attained (c). (Figure adapted from reference [5])

labeling strategy. First, the half-life of the isotope sets a practical limit to the maximum theoretical molar activity, the radioactivity per mole (usually expressed in gigabecquerels per micromole, GBq μmol^{-1}), of the isotope that can be produced as shown in Eq. 3, where N is Avogadro's number.

$$\text{molar activity}_{\max} = N \times \frac{\ln 2}{t_{1/2}} \quad (3)$$

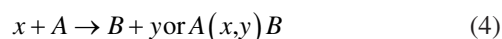
Second, as a guideline, the radiosynthetic procedures and purification of the radiolabeled tracer should be completed within ≈ 2 half-lives of the isotope to ensure meaningful molar activity (radioactivity per amount, usually expressed in gigabecquerels per micromole, GBq μmol^{-1}) of the radiolabeled product for in vivo studies. Therefore, in order to obtain maximal molar activity radiolabels are best introduced late in the radiosynthesis, which is often achieved by the use of a *prosthetic group*, a radiolabeled precursor that can be conjugated to the nonradioactive target molecule or material using fast and selective chemistry preferably in a single step [6]. Third, the half-life of the radioisotope constrains the timeframe over which the passage of the radiolabeled compound can be tracked in vivo. For this purpose, the physical half-life of the radioisotope should be matched to the *biological* half-life of the vector, in this case the nanosystem. This is perhaps best illustrated by the case of radiolabeled antibodies, which have biological half-lives in the order of days, and consequently only longer-lived isotopes such as zirconium-89 (^{89}Zr , $t_{1/2} = 78.41$ h), indium-111 (^{111}In , $t_{1/2} = 2.80$ d), iodine-124 (^{124}I , $t_{1/2} = 4.18$ d), and iodine-131 (^{131}I , $t_{1/2} = 8.03$ d) can be used for the tracking of directly labeled antibodies. Other important concepts in the radiopharmaceutical development are the molar activity mentioned already earlier, specific activity, radiochemical yield, and radiochemical purity, the definitions of which will be reviewed next. The field of radiopharmaceutical chemistry today follows a consensus nomenclature compiled by Coenen *et al.* and set forward in 2017 [7].

The molar activity of a radiolabeled compound is defined as the amount of radioactivity per mole of compound, whereas *specific activity* refers to the amount of radioactivity per mass, most often denoted in GBq mg^{-1} or MBq mg^{-1} . In most cases the exact molecular weight of the nanosystem is not known or reported, thus the specific activity gives a more meaningful denotation on how much radioactivity is incorporated to the nanosystem. Furthermore, if the final radiolabeled product contains a nonradioactive starting material which cannot be removed, as is the case for most nanomaterials, the terms *apparent molar activity* and *apparent specific activity* should be used. The term *radiochemical yield* refers to the quantity (often expressed in percentage of the starting quantity) of the radioisotope incorporated to the radiolabeled product. Although analogous to chemical yield, an important

notion of the radiochemical yield is that it needs to be always calculated using starting and final values for the same radioisotope which have been decay-corrected to the same point in time, typically, for example, the end of synthesis (EOS) or the end of bombardment (EOB) for the nuclear reaction producing the radioisotope. The term *radiochemical purity* in turn is analogous to chemical purity and is used to describe the purity of the product with respect to the presence of other radiolabeled compounds in the final product, again decay-corrected to a fixed point in time. Typically, radiochemical purities exceeding 95% are considered adequate in terms of in vivo applications, but this level depends on the identity and pharmacokinetics of the impurity and more stringent criteria to radiochemical purity might need to be applied accordingly.

2.2 Nuclear Reactions for Radionuclide Production

All the radionuclides used in nuclear medicine are artificially manufactured through nuclear reactions of stable isotopes. The production of radionuclides is commonly carried out using either particle accelerators or nuclear reactors. In radionuclide production, a nucleus of a stable element (the “target”) is bombarded with nucleons (protons and neutrons) or other nuclei of stable elements, such as helium and deuterium (the “projectile”). The target and the projectile react, forming a product nucleus. In most cases, the primary product nuclei formed in the reaction are in an excited state and further emit out nucleons, small nuclei, or gamma radiation (the “ejectile”) to form the final product nucleus. The nuclear reactions are represented by the notation.



where x is the projectile, A is the target, B is the final product after the reaction, and y is the ejectile. Typical reactions used in the radionuclide production are presented in Fig. 4.

The nuclear reactions require energy enough to bring the positively charged projectile and target in contact over the repulsive Coulomb forces (“Coulomb barrier”). On the other hand, the possibly negative reaction Q value, that is, the difference of the masses before and after the nuclear reaction needs to be compensated by a proper projectile energy for enabling the reaction. These two energies define the minimum projectile energy needed for a nuclear reaction.

The probability for certain nuclear reaction to happen is called cross section. A unit of a cross section is called “barn” (b) and $1 \text{ b} = 10^{-28} \text{ m}^2$. Therefore, the cross section can be thought as an area that the projectile needs to hit – the larger the area, the more probable the reaction is. Cross section is

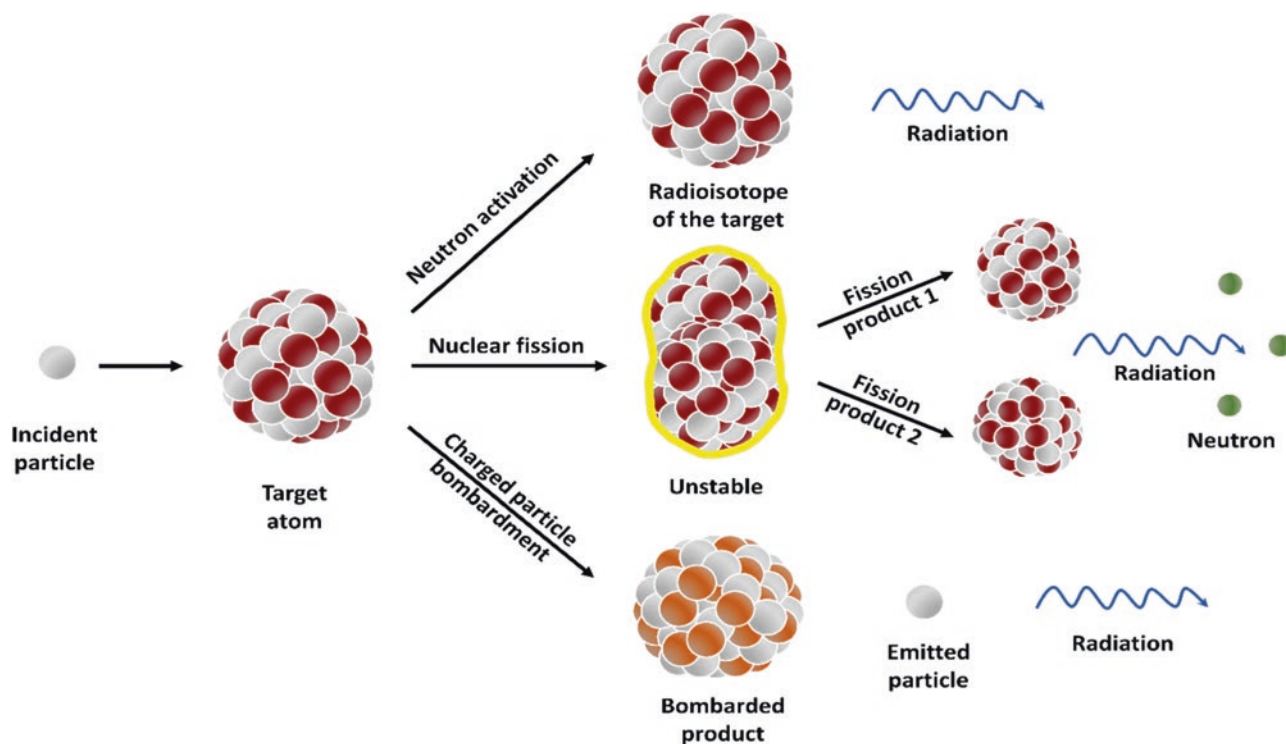


Fig. 4 The most common nuclear reactions in radionuclide production. Neutron activation and nuclear fission are carried out in nuclear reactor while high-energy charged particle bombardment is carried out in accelerators

defined for all the reaction types separately, and it is dependent on the energy of the projectile. Therefore it is important to select an optimal energy for the projectile from the point of view of maximizing the production of the nuclide of interest and minimizing the side reactions leading to impurities. In practice, the target material can be in gaseous, liquid, or solid form. Important things in target design are to ensure a safe manipulation of a highly active target after the irradiation, and to have methods to separate the produced activity from the target material.

Different kinds of charged particles needed for nuclear reactions (e.g., protons, deuterons, and alpha particles) are formed and accelerated in particle accelerators. One most typical of them in radionuclide production is a cyclotron, where the protons are accelerated in the spiraling path. Typical nuclei produced with accelerators are, for example, yttrium-86 (via reaction $^{86}\text{Sr}(p,n)^{86}\text{Y}$), indium-111 ($^{112}\text{Cd}(p,2n)^{111}\text{In}$), gallium-67 ($^{67}\text{Zn}(p,n)^{67}\text{Ga}$), and fluorine-18 ($^{18}\text{O}(p,n)^{18}\text{F}$). For reactions requiring neutrons (e.g., radiative capture (n,γ) and fission), usually pool-type research nuclear reactors are used. In many reactions, especially in radiative capture, thermal neutrons, that is, the neutrons with a speed of about 2000 m/s are utilized. These reactions are used, for example, in production of strontium-89 ($^{88}\text{Sr}(n,\gamma)^{89}\text{Sr}$), technetium-99 ($^{98}\text{Mo}(n,\gamma)^{99}\text{Tc}$), and lutetium-177 ($^{176}\text{Lu}(n,\gamma)^{177}\text{Lu}$). Also (n,p) and (n,α) reactions can be utilised, as well as reactions proceeding through a short-lived intermediate product that decays to the desired radioisotope,

such as iodine-131 which is produced via first making tellurium-131 in $^{130}\text{Te}(n,\gamma)^{131}\text{Te}$ reaction, and then letting the ^{131}Te ($t_{1/2} = 25$ min) to decay by β^- emission to ^{131}I . In nuclear fission reactions ($n,\text{fission}$) neutron splits a heavy nucleus in two pieces with few neutrons emitted in process. Fissions induced by thermal neutrons are resulting in an antisymmetric split with one heavier and one lighter mass nucleus. The commonly used target materials in fission reactions are uranium-235 (^{235}U) and plutonium-239 (^{239}Pu). The most relevant fission products in nuclear medicine are ^{131}I for theranostic applications and ^{99}Mo for the use as radioactive parent in $^{99}\text{Mo}/^{99\text{m}}\text{Tc}$ generators.

Radioisotope production is globally concentrated on facilities with accelerators and reactors. Smaller medical cyclotrons capable for the production of short-lived positron emitters (^{11}C , ^{13}N , ^{15}O , ^{18}F , ^{89}Zr , ^{124}I) are available at academic institutions and hospitals to account for the use of these isotopes in the clinic and the fact that some of them cannot be transported due to the short half-lives (<2 hours). Additionally, $^{99}\text{Mo}/^{99\text{m}}\text{Tc}$ and $^{68}\text{Ge}/^{68}\text{Ga}$ generators are nowadays nearly ubiquitous in research and hospital laboratories because of their long usable life time which allows the users to dispense the radioisotope on demand. Longer-lived radioisotopes can be purchased through a number of vendors worldwide or acquired through academic collaborations in the case of more rare radioisotopes.

2.3 Principles for the Safe Handling of Radioactive Materials

Working safely with radioactivity requires a number of precautions and specialized working areas which are usually shared between many researchers at a given institute. The type of laboratory and shielding needed and the safe handling practices employed depend on the radioisotope and the amount of radioactivity that needs to be handled at one time. The type of the work also matters as some tasks such as radiotracer administration to animals carry a greater risk of personnel exposure than, for example, the measurement of excised tissue samples in sealed tubes. Safe practices in working with radioactivity need to be followed at every step of the process from the radiolabeling synthesis to biological evaluation to disposal and storage of radioactive waste. The respective national and institutional regulations and guidelines are reviewed during introductory training on radiation safety and the radiation safety officer or department at the institute ensures personnel compliance by offering guidance and continued training. Dose monitoring needs to be offered to personnel working with radioactivity and medical clearance is most often needed prior to starting the work. As a general guideline, the amount of radiation dose accumulated during a procedure can be greatly reduced by using appropriate physical shielding (e.g., a fume hood with a lead-glass window or a remotely controlled synthesis apparatus), by increasing the distance from the radiation source (e.g., by handling radioactive vials with tongs or manipulators), and by minimizing the time spent handling the radioactive source (e.g., by careful planning of the procedure and practicing with mock runs with nonradioactive reagents). Additionally, the benefit gained using radioisotopes should always outweigh the risks associated with their use and the amount of radioactivity used should be kept as low as reasonably possible.

2.4 Radiometric Detection Methods and Nuclear Imaging

The inherent properties of radioactivity contribute to the superior detection sensitivity and ease of quantitation for radiometric methods. First, as most of the radioisotopes employed in radiopharmaceutical development are rare or nonexistent in natural systems as they have been artificially produced in nuclear reactions, there is no “natural” radioactive signal with the same energy spectrum that could hamper the analysis. Naturally abundant radioactive isotopes of elements such as potassium-40 (about 0.012% of natural potassium is ^{40}K) will of course be present in biological samples, but the levels are several orders of magnitude lower to any injected radiotracer and can be excluded from the analysis based on the spectra of the emitted radiation. Second, the aforementioned energy spectra allow for the identification of

the desired radionuclide in a mixture of radionuclides and background radiation, enabling the detection of two or more isotopes at the same time if the energies emitted by the isotopes are sufficiently different. Semiconductor gamma spectrometers of superior energy resolution are most often used in these applications. Finally, the number of radioactive disintegrations detected over a given time (*count rate*) is directly proportional to the number of radioactive atoms in the sample which greatly simplifies the quantification.

The quantification of radioactivity is relatively straightforward with radioisotopes emitting highly tissue-penetrant gamma radiation as this can be detected and quantified with minimal sample processing. The radioactivity content in excised tissue samples is, for example, determined simply by measuring the radioactivity in the freshly collected tissue using an automated gamma counter. The commercially available automated counters are the workhorses of both clinical and academic radiochemistry laboratories as they have a large sample handling capacity with automated sample changing, facile operation and robust well-type thallium-doped sodium iodide NaI(Tl) detectors which usually require minimal maintenance over their lifetime. With all radiation detection systems, one needs to take into account the fact that the systems are saturable. This means that the response of the detection system remains linear only over a certain radioactivity range and at activities exceeding this range the response of the detection system deteriorates. The reason for this is the detection system dead time, that is, the time the system remains unresponsive and thus unable to detect the radiation after detection of a radiation event. Care must therefore be taken to maintain the sample activities at the linear range of the detection system. Radioisotopes which do not emit any usable gamma radiation for detection purposes are rare especially in theranostic systems, but if needed, liquid scintillation counting offers a convenient detection method for low-energy β - and α -emitting radioisotopes in biological samples. As the name implies, liquid scintillation counting relies on the detection of the light generated by the absorption of the energy emitted by the radioisotope in the scintillation medium, referred to as a cocktail. The liquid scintillation cocktails are commercially available solutions of solvents capable of absorbing the energy of the emitted radiation and organic scintillator molecules which in turn emit visible light in response to transfer of the energy from the solvent to the scintillator molecule. Unsurprisingly, energy-rich aromatic ring structures and oxazoles compose the backbone for both solvent and scintillator molecules in commercial cocktails. The sample preparation for liquid scintillation counting is slightly more complicated than that for gamma counting, as the homogenized tissue samples need to be solubilized to the solvent and the sample rendered colorless by the addition of, for example, hydrogen peroxide. The sample composition, particularly color and certain compounds, can greatly affect the intensity of the detected light through quenching.

Nuclear imaging refers to the detection of gamma radiation emitted by a radioisotope outside of the living subject and subsequent process of reconstruction of the measured radioactivity distribution to an image. For nuclear imaging in diagnostic purposes, the radioisotope must have gamma emissions, these can either be the two coincident 511-keV annihilation gammas of positron emitters, or single-energy gamma quanta emitted by other isotopes. The former are detected using a technique called positron emission tomography (PET) and the latter by single-photon emission computed tomography (SPECT). The principles of image formation in PET and SPECT imaging are outlined in Fig. 5. Both PET and SPECT are fully translational imaging modalities, meaning that the tracer design, imaging system and setup are the same in small laboratory animals and in the clinic. The instrument design obviously varies as the systems are miniaturized for the imaging of laboratory rodents under inhalation anesthesia, but the detection principle and the study workflow remain the same. Since the molar activity of radiotracers is typically high, they can be administered in doses significantly lower than those used to elicit a pharmacological response. This makes it possible to use expensive and potentially harmful or even toxic substances *in vivo* without disturbance to the system under study. This *microdosing principle* [8] has made possible the investigational use of radiotracers early on in the drug development pipeline to study the target engagement and elimination of new drugs. For theranostic nanosystems the microdosing principle might not in all cases be directly applicable, as a macrodose of the nanomaterial might be needed for concomitant drug

delivery. Nevertheless, the high molar activity of radioisotopes means that they can be used in the radiolabeling reactions in minute amounts and thus with minimal influence on the physicochemical properties of the nanosystem. A caveat in nuclear imaging modalities is the fact that they do not provide any anatomical information on the localization of the tracer except for what can be deduced from the tracer accumulation to nontarget organs and knowledge on their location in the body. Therefore, co-registration of the nuclear image with an image obtained using another imaging modality, for example, X-ray computed tomography (CT) or magnetic resonance imaging (MRI) is often necessary for the precise delineation of the sites of radiotracer accumulation. Conveniently, the large molecular weight of nanomaterials allows for the incorporation of both the radiolabel and a contrast agent for CT or MRI to be incorporated to the same construct, generating a *multimodality* tracer.

3 Radiolabeling Strategies

3.1 Radiometals

Radiometals are radioactive isotopes of metal elements which have become an important tool for radiopharmaceutical drug development in nuclear medicine. Radiometal labels have been employed for a multitude of radiotracers from radiometal-labeled small molecules to peptides, antibodies, and nanoparticles. Radiometal labeling strategies have several advantages over other radiolabeling techniques, for

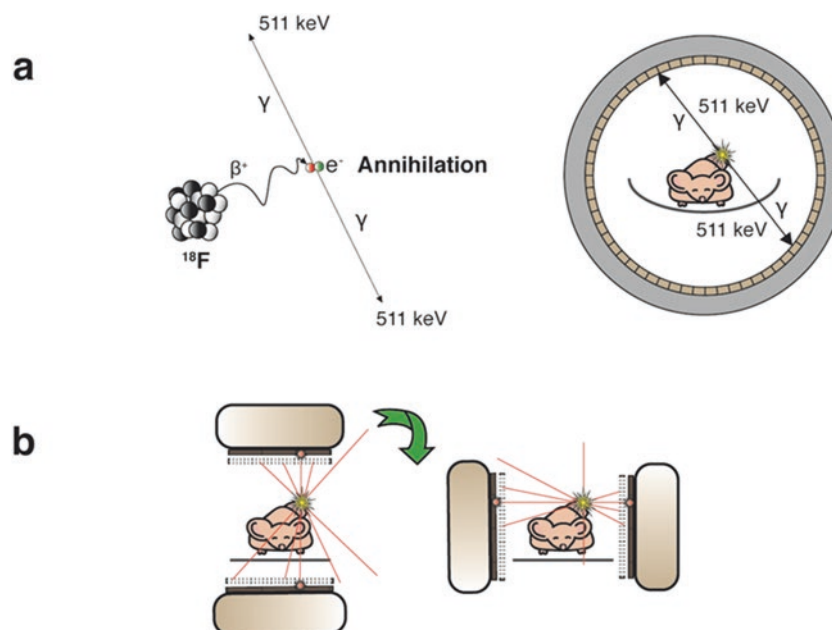


Fig. 5 The principle of detection for positron emission tomography (PET) and single-photon emission computed tomography (SPECT). In PET (a), the detectors are arranged on a ring around the subject, and the coincident 511-keV gamma rays from the positron annihilation are detected. In SPECT (b), the tomographic image is generated by revolving an array of detectors and a collimator around the subject, and only the gamma quanta which are directly perpendicular to the collimator will pass through to the detectors for registration

example, the easy commercial availability of many radiometals, the pairs of diagnostic and therapeutic radionuclides of the same element, high specific activity, and in often cases favorable radiation dosimetry. The most relevant radiometal isotopes and their properties for SPECT, PET, and theranostics in the clinical and preclinical research have been listed in Table 1.

3.1.1 Chelator-Mediated Radiolabeling with Radiometals

The conjugation of radiometals to radiopharmaceuticals is typically achieved by chelation, the coordination of the radiometal cation by a chelating agent. In order to use the radiometals in biological applications, the radiometal cation must form a stable complex with the chelator to avoid undesirable hydrolysis and transchelation (the displacement of the radiometal by other metal ions in chelator cavity) in vivo. For conjugation to

the targeting vector, a number of bifunctional chelating agents (BFCs) have been designed and developed. BFCs generally contain nitrogen (N) and oxygen (O) atoms in their structures that can donate an electron pair to form dative covalent bonds with the metal ions. Moreover, at least one side chain of the BFCs is usually modified with a functional group that can be covalently conjugated to the targeting molecules. The functional groups attached to the carbon backbone of the chelators are preferable due to the availability of all of the N and O atoms for the radiometal coordination, resulting in better stability of metal-chelator complex. A radiometal-labeled radiopharmaceutical consists of three parts: the chelating agent that forms complexes with radiometals, the spacer or linker that is covalently coupled between the chelate and the vector in order to keep the often charged radiometal complex away from the target binding motive, and the biomolecule or targeting vector, such as an antibody, peptide, or nanoparticle (Fig. 6).

Table 1 Overview of radiometals for SPECT, PET, and theranostics

Metal	Radioisotope	Half-life ($t_{1/2}$)	Decay mode	β_{\max} MeV (% intensity)	γ keV (% intensity)	Imaging modality	Production method
Scandium (Sc)	^{44}Sc	3.97 h	β^+/EC	1.474 (94.27)	1157 (99.9)	PET	Cyclotron
	^{47}Sc	3.3492 d	β^-	0.600 (31.6)	159.38 (68.3)	SPECT/ theranostic	Cyclotron
Copper (Cu)	^{61}Cu	3.339 h	β^+/EC	1.216 (51)	282.96 (12.2) 656.01 (10.8)	PET	Cyclotron
	^{62}Cu	9.67 m	β^+/EC	2.937 (97.6)	–	PET	Generator
	^{64}Cu	12.701 h	$\beta^+/\beta^-/\text{EC}$	0.653 (17.6)	511 (35.2)	PET/ theranostic	Cyclotron
	^{67}Cu	61.83 h	β^-/γ	0.377 (51)	91.27 (7) 93.31 (16.1) 184.58 (48.7)	SPECT/ theranostic	Cyclotron
Gallium (Ga)	^{66}Ga	9.49 h	β^+/EC	4.153 (51)	833.53 (5.9) 1039.22 (37) 2751.84 (22.7)	PET	Cyclotron
	^{67}Ga	3.262 d	EC/γ	–	93.31 (38.81) 184.58 (21.41) 300.22 (16.64) 393.53 (4.56)	SPECT	Cyclotron
	^{68}Ga	67.71 m	β^+/EC	1.899 (87.72)	–	PET	Generator
Rubidium (Rb)	^{82}Rb	1.258 m	β^+/EC	2.601 (13.13) 3.378 (81.76)	776.52 (15.08)	PET	Generator
Yttrium (Y)	^{86}Y	14.74 h	β^+/EC	1.221 (11.9)	443.13 (16.9)	PET	Cyclotron
	^{90}Y	64 h	β^-	2.280 (99.99)	–	SPECT/ Theranostic	Generator
Zirconium (Zr)	^{89}Zr	78.41 h	β^+/EC	0.902 (22.74)	909.15 (99.04)	PET	Cyclotron
	^{97}Zr	16.749 h	β^-/γ	1.916 (87.8)	743.36 (93.09)	SPECT/ theranostic	Reactor
Technetium (Tc)	$^{94\text{m}}\text{Tc}$	52 m	β^+/EC	1.592 (8.9) 1.938 (4.1) 2.438 (67.6) 3.460 (12.8)	871.091 (94)	PET	Cyclotron
	$^{99\text{m}}\text{Tc}$	6.01 h	IT	–	140.51 (89)	SPECT	Generator
Indium (In)	^{111}In	2.8047 d	EC/γ	–	171.28 (90.7) 245.35 (94.1)	SPECT	Cyclotron
Lutetium (Lu)	^{177}Lu	6.647 d	β^-/γ	0.177 (11.61) 0.4983 (79.4)	112.95 (6.17) 208.37 (10.36)	SPECT/ theranostic	Reactor

Data retrieved from the NuDat2 database, <http://www.nndc.bnl.gov/nudat2>

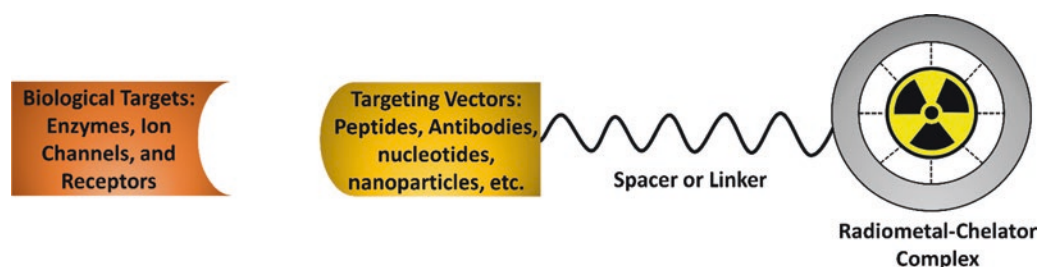


Fig. 6 The general design of radiometal-labeled radiopharmaceuticals

The physical and chemical properties of the radiometal-chelator complex affect the overall pharmacokinetic properties of the radiolabeled compounds. Most of the radiometal-chelator complexes are very hydrophilic and have a positive charge leading to rapid clearance from the biological system through renal excretion. Therefore, the chelating agent and the radiometal must be carefully matched to tailor the complex stability and charge. In general, the radiometal-chelator pair is selected based on the chelating agent and radionuclide properties, for example, ionic charge, ionic radius, cavity size in the chelator, the number of donor binding groups, and the rate of metal complex formation and dissociation. Table 2 shows the currently used radiometal chelators and their bifunctional derivatives, and the appropriate radiometal and typical radiolabeling conditions [9]. Since it is preferable to conjugate the chelator to the nanosystem before the radiometal complexation to avoid losses of radioactivity, the radiolabeling condition is as important as other factors mentioned previously as the construct needs to withstand the radiolabeling conditions. Room temperature and neutral pH conditions are superior when the labeled molecules are heat and pH sensitive, such as in the case of nucleotides and antibodies. Moreover, the labeling time is crucial when working with short half-life radiometals, such as scandium-44 (^{44}Sc), copper-62 (^{62}Cu), ^{68}Ga , rubidium-82 (^{82}Rb), and $^{94\text{m}/99\text{m}}\text{Tc}$. Thus, the coordination kinetics must be fast (5–15 min reaction times) and yield high radiolabeling efficiency. Macrocyclic chelators, having inherently constrained geometries where the coordinating groups are close to another creating a “scaffold” metal ion binding sites, undergo only minor conformational and loss in entropy upon radiometal coordination. In contrast, acyclic chelators such as desferrioxamine (DFO) must undergo a more drastic change in their geometry in order to arrange the donor atoms to coordinate with the metal ion [9]. However, despite this thermodynamic favorability of radiometal coordination to macrocycles, they generally require heating (60–90 °C) and longer reaction times (>30 min) to attain radiolabeling at a reasonable yield. In acyclic chelators the coordination often occurs at room temperature within 15 minutes. The radiometal-chelator complex stability should be validated in terms of thermodynamic stability, possibility of transchela-

tion (e.g., Fe^{3+} , EDTA, and DTPA), acid catalyzed dissociation, and stability in physiological conditions relevant to the administration route.

Overall, several factors need to be taken into consideration when designing chelator-mediated radiolabeling of theranostic nanosystems. The choice of the radiometal is the foremost consideration as the physical half-life should be matched to the timeframe of the experiment and the nuclear properties to the theranostic application. From the standpoint of the radiometal-chelator complex, the stability in vitro and in vivo, the radiolabeling conditions (media, pH, time, and temperature), and the conjugation chemistry available for nanosystem labeling all need to be taken into account.

3.1.2 Chelator-Free Radiolabeling

Chelator-based radiometal labeling has been widely employed in nuclear imaging and radiotherapeutic development with radiometals. However, a number of challenges in the chelator-based radiolabeling approach still remain. First, the nanomaterials may not be able to tolerate the severe radiolabeling conditions, such as acidic pH and high temperature, leading to instability and destruction. Second, the incorporation of the hydrophilic chelator onto the surface of nanosystems can change their overall pharmacokinetics, surface charge, and hydrodynamic size, resulting in completely different properties from the native vector. Moreover, the coordination chemistry is vastly different between different chelators and radiometals necessitating a careful evaluation of radiometal and chelator suitability for the application. However, as radiometals can be directly coordinated to certain functional groups that either intrinsically exist in the nanoparticle structure or that are grafted on the surface of nanoparticles, chelate-free strategies have shown potential to maintain the native properties of the nanoparticles in a way that better reflects the behavior of nonradiolabeled nanoparticles in vivo.

Several approaches to chelate-free radiolabeling of nanoparticles have been proposed to match different nanoparticle surface characteristics and modifications. Chelator-free [^{64}Cu]CuS nanoparticles have been developed as a platform for the simultaneous PET/CT imaging and photothermal therapy [10]. The [^{64}Cu]CuS can be formed by direct synthe-

Table 2 Common radiometal chelators, their derivatives, relevant radiometal ions, and radiolabeling conditions

Type	Chelator	Common derivatives	Radiometal ions	Radiolabeling conditions
Acyclic chelators	<p>Desferrioxamine (DFO)</p>	<p><i>p</i>-SCN-Bn-DFO</p> <p>Bifunctional DFO, R = amide, NHS ester, etc.</p>	$^{67/68}\text{Ga}^{3+}$ $^{89}\text{Zr}^{4+}$	25 °C 30–60 min pH 3.5–7.3
	<p>Diethylenetriaminepentaacetic acid (DTPA)</p>	<p><i>p</i>-SCN-Bn-1B-DTPA</p> <p><i>p</i>-SCN-Bn-1B4M-DTPA</p> <p>CHX-A''-DTPA</p>	$^{44/47}\text{Sc}^{3+}$, $^{111}\text{In}^{3+}$, $^{177}\text{Lu}^{3+}$ $^{86/90}\text{Y}^{3+}$	25–75 °C 5–60 min pH 5–5.5
		<p><i>p</i>-SCN-Bn-CHX-A''-DTPA</p>		

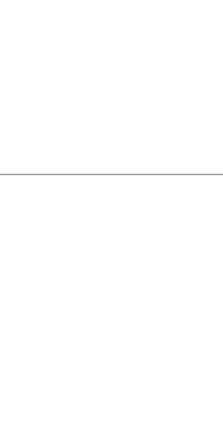

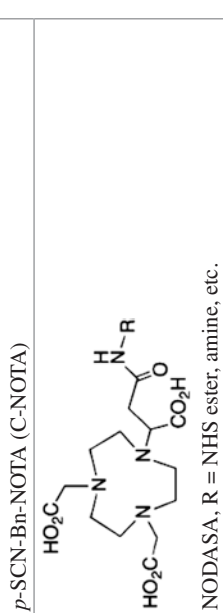
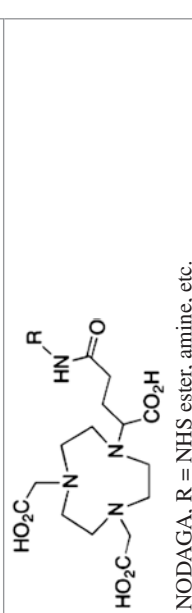
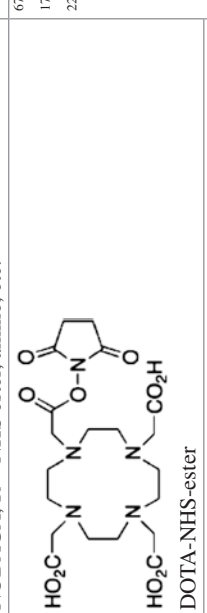
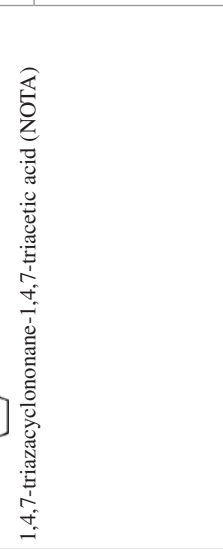

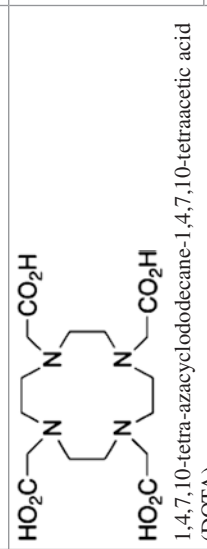

<p>Macrocyclics</p>	 <p>1,4,7-triazacyclononane-1,4,7-triacetic acid (NOTA)</p>	 <p><i>p</i>-SCN-Bn-NOTA (C-NOTA)</p>	<p>$^{64}\text{Cu}^{2+}$, $^{67/68}\text{Ga}^{3+}$, $^{44/47}\text{Sc}^{3+}$, $^{111}\text{In}^{3+}$, $^{177}\text{Lu}^{3+}$, $^{86/90}\text{Y}^{3+}$</p>	<p>25–95 °C 5–60 min pH 4–6.5</p>
 <p>NODASA, R = NHS ester, amine, etc.</p>	 <p>NODAGA, R = NHS ester, amine, etc.</p>	 <p>DOTA-NHS-ester</p>	<p>$^{67/68}\text{Ga}^{3+}$, $^{44/47}\text{Sc}^{3+}$, $^{111}\text{In}^{3+}$, $^{177}\text{Lu}^{3+}$, $^{86/90}\text{Y}^{3+}$, $^{212}\text{Pb}^{2+}$, $^{225}\text{Ac}^{3+}$</p>	<p>25–90 °C 10–120 min pH 4–6</p>
 <p>1,4,7,10-tetra-azacyclododecane-1,4,7,10-tetraacetic acid (DOTA)</p>	 <p><i>p</i>-SCN-Bn-DOTA</p>	 <p>DOTAGA, R = amide, NHS ester, etc.</p>	 <p>DOTAGA-anhydride</p>	<p>(continued)</p>

Table 2 (continued)

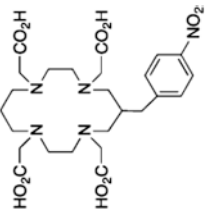
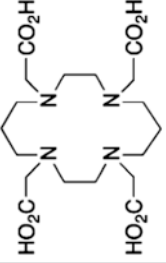
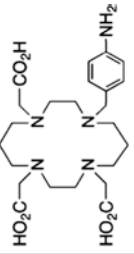
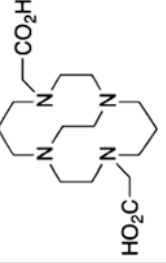
Type	Chelator	Common derivatives	Radiometal ions	Radiolabeling conditions
	 <p>1,4,8,11-tetra-aza-cyclotetradecane-1,4,8,11-tetraacetic acid (TETA)</p>	 <p><i>p</i>-NO₂-Bn-TETA (C-TETA)</p>  <p><i>p</i>-NH₂-Bn-TE3A</p>  <p>CB-TE2A</p>	⁶⁴ Cu ²⁺	25–95 °C 60 min pH 5–7

Table adapted from reference [9]

sis from the radioactive precursor in which the ^{64}Cu is incorporated into the building block of CuS and a high radiolabeling yield was achieved. A similar direct radiolabeling approach has been documented in monoclonal antibody radiolabeling with rhenium-188 for radioimmunotherapy [11]. The protein disulfide bridges are firstly reduced with different reducing agents, generating thiol groups (R-SH) that can coordinate with reduced oxidation state of $[\text{Re}^{2+}\text{ReO}_4^-]$ in the presence of stannous chloride (SnCl_2) as a reducing agent.

The heat-induced radiolabeling (HIR) of radioactive cations has been employed in the radiolabeling of superparamagnetic iron oxide nanoparticles [12–14]. The thermal stability of iron oxide nanoparticles allows the high heat activation of the iron oxide core to coordinate with radiometals (e.g., ^{64}Cu , ^{89}Zr , ^{111}In , and ^{59}Fe) without changing the structure, magnetic properties, and size of the nanoparticles. In addition, the selective binding of radiometals to the surface of nanoparticles has been reported. The layered double hydroxide (LDH) nanoparticles have demonstrated the potential to be readily radiolabeled with radiometals without the aid of chelators [15]. Bivalent and trivalent cations (e.g., $^{64}\text{Cu}^{2+}$ and $^{44}\text{Sc}^{3+}$) can form stable coordination with high labeling efficiency into the brucite-like cationic layers of the LDH, while the tetravalent cation such as $^{89}\text{Zr}^{4+}$ cannot efficiently label onto the LDH layer due to the lack of compatibility between the ionic radius and the LDH crystal structure. Also, a similar strategy has been applied to investigate the stereotype of chelator-free radiolabeling nanographene with ^{64}Cu [16]. The reduced graphene oxide (RGO) exhibits a superior intrinsically ^{64}Cu radiolabeled to the nanographene due to the transition metal- π -electron interaction where the electron transfer takes place between $^{64}\text{Cu}^{2+}$ and π -bond, providing an alternative approach to maintain the properties of nanographene in vivo. The direct implantation method of theranostic radiolanthanoid, dysprosium-159 (^{159}Dy) to thermally hydrocarbonized porous silicon (THCPSi) nanoparticles has been reported [17]. The THCPSi substrates are irradiated with radioactive ion beam (RIB) of ^{159}Dy at the intensity of 10^{10} particles over 39 h, resulting in the implantation of ^{159}Dy ions on the mesoporous layer substrate. The $[\text{Dy}^{159}\text{THCPSi}]$ nanoparticles demonstrated good stability in vivo after 7 days of intratumoral administration as the ^{159}Dy remained embedded in THCPSi nanoparticles inside the tumor, prompting the use of other RIB-based radiolanthanoids for chelator-free radiolabeling with mesoporous nanoparticles. Overall, the chelator-free radiolabeling strategies reveal the potential of alternative approaches for radiolabeling with radiometals. However, understanding of the coordination mechanism between the radiometal and the nanoparticle itself as well as the stability of the radiometal complex are always warranted before in vivo applications.

3.2 Radiohalogenation

Radiohalogenation can be performed using typical organic chemistry techniques such as nucleophilic and electrophilic substitution. The chemistry is chosen such that the new bond is strong enough to withstand physiological conditions. The carbon-halogen bond energy decreases with increase in size of halogens from $\text{F}^- < \text{Cl}^- < \text{Br}^- < \text{I}^-$. The bond strength increases with increasing number of π bonds of the carbon. Aromatic carbon-halogen bonds have higher bond strengths compared to the aliphatic counterparts with hybridization. This makes radioiodination on aromatic substrates less prone to hydrolysis and β -elimination. Direct radioiodination technique uses electrophilic and nucleophilic substitutions as well as electrophilic addition to unsaturated compounds in certain cases.

Electron rich aromatic compounds such as those containing the activating hydroxyl, amine and methoxy functionalities can be radioiodinated using electrophilic aromatic substitution. The substitution of the hydrogen at the ortho or para positions relative to the activating groups is called iododeprotonation. The ortho and para positions relative to the electron donating group are substituted due to the higher delocalization of charge in the transition state as shown in Fig. 7 for the dopamine D_2 receptor radioligand, IBZM.

For less activated aromatic rings, the synthesis is carried out in two steps with the formation of an activated derivative followed by the substitution with an electropositive radioiodine. The most commonly used organometallic precursors for iododemetalation are alkylstannyl compounds along with silyl and boronic acid derivatives. Carbon-metal bond is more activated for an electrophilic attack than a carbon-hydrogen bond. The drawback of using tri-alkyltin derivatives is the toxicity of tin compounds. Silyl derivatives are less toxic, a desirable property when the radioiodinated compound is to be used for in vivo studies. The silicon-carbon bond is stronger than tin-carbon bond which results in slower reaction rates for iododesilylation. Boron derivatives also have low toxicity and boron compounds such as boronate

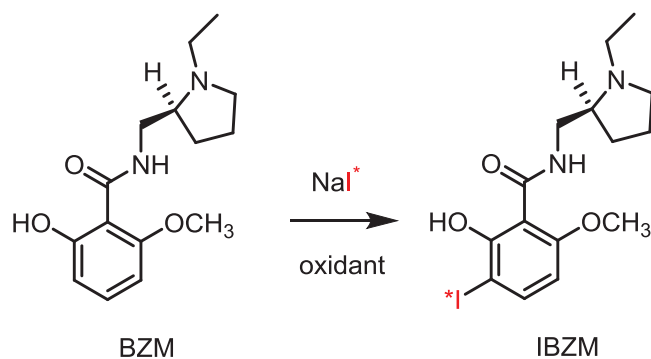


Fig. 7 Iododeprotonation of BZM

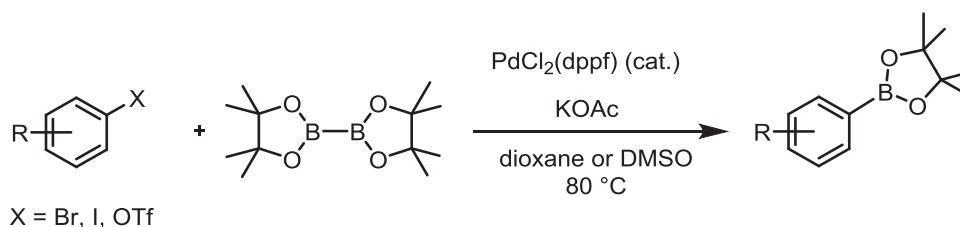


Fig. 8 Miyaura borylation reaction

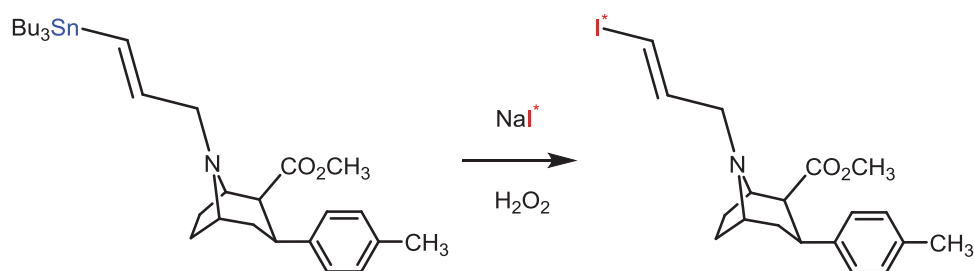
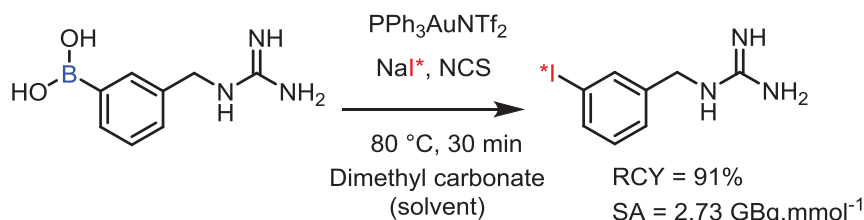


Fig. 9 Synthesis of [¹³¹I]MIBG using iododeboration (top) and PE2I using iododestannylation (bottom)

esters and trifluoroborate salts are air stable crystalline solids making them ideal precursors for halodemallation reactions [18]. The boronate esters and trifluoroborate salts can be regioselectively prepared using the Miyaura borylation reaction which is the coupling of the bis(pinacolato)diboron with aryl/vinyl halides using palladium catalyst as shown in Fig. 8. Mild basic conditions for the borylation reaction is crucial to prevent activation of the borylated product and undergo Suzuki coupling reaction [19]. The ipso substitution of the metal with the iodine is regioselective under mild oxidative conditions. [¹³¹I]MIBG has been prepared using iododeboration as shown in Fig. 9.

The radioiodine is generally obtained as sodium iodide. It has to be oxidized to its unipositive charged state for electrophilic reactions. It can be oxidized using water soluble oxidants such as chloramine-T, N-chlorosuccinimide (NCS), and peracids [20]. Chloramine-T is a strong oxidant but may lead to by-products. Low reaction temperatures and fresh reagents are key to successful oxidation. Polymer bound chloramine called Iodobeads [21] have been developed to reduce the exposure of oxidant sensitive molecules. Iodogen is another chlorine-based oxidant but it is milder and hence can be used with proteins and peptides. Iodogen is water insoluble and it is typically used as a thin film on a glass vial. Iodogen is compatible with common detergents which makes it widely applicable for labeling biologics. Radiolabeled proteins have been shown to have different stabilities depending on the

source of the oxidizing agent showing there are fundamental differences among the mechanisms of radioiodination [22]. Structure of some of the oxidants is shown in Fig. 10.

Radioiodination conditions are harsh for sensitive molecules such as peptides and antibodies. To prevent such exposure, indirect radiolabeling methods are used in which prosthetic groups such as Bolton-Hunter reagent are radioiodinated, which can then be conjugated to biomolecules [23]. A typical conjugation of a radioiodinated Bolton-Hunter reagent is shown in Fig. 11. Other spacers which are bifunctional and can be used for radioiodination are shown in Fig. 12. These allow versatile bioconjugation to sulfhydryl and amine containing compounds.

Nucleophilic substitution is carried out in compounds which are functionalized with electron-withdrawing groups where the carbon is functionalized with good leaving groups such as mesylate, triflate, tosylate, or brosylate as shown in Fig. 13.

Aliphatic carbons can use either S_N1 or S_N2 mechanisms and aromatic compounds use S_NAr mechanism. The rate-determining step for a S_NAr reaction is the attack of the nucleophile and formation of the intermediate complex. For increasing the reaction rate, the labeling position needs to be activated by electron withdrawing groups such as -NO₂, aldehyde, ketone, ester, and amide in the ortho- or para-positions or catalyzed by metal salts such as Cu-salts.

For aryl amines the classic Sandmeyer-type reaction can be performed by diazotization of the amine, followed by

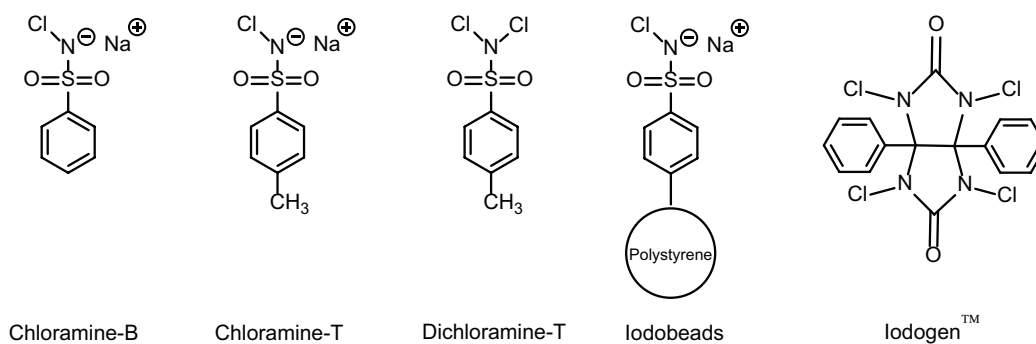


Fig. 10 Structure of some chlorine-based oxidants

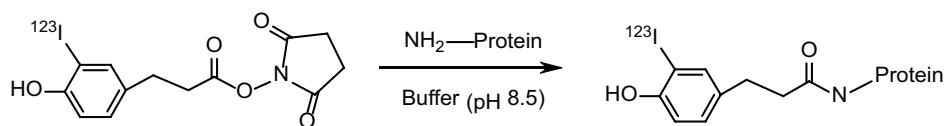


Fig. 11 Conjugation of a protein to a radioiodinated Bolton-Hunter reagent

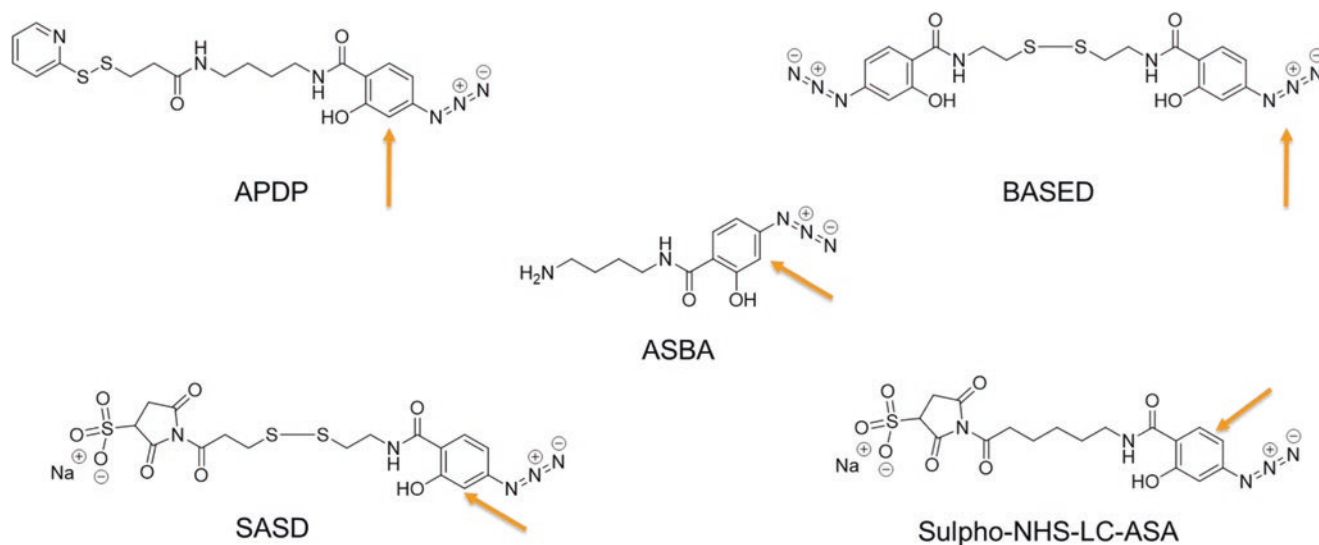


Fig. 12 Spacers which can be radioiodinated; radioiodination positions have been marked

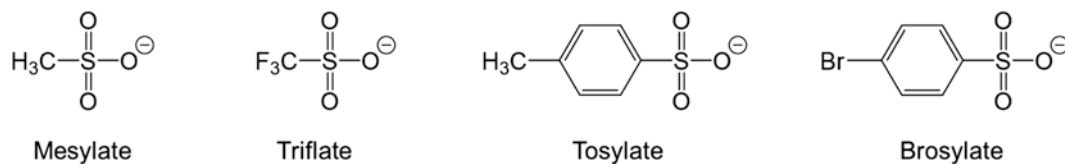


Fig. 13 Structure of leaving groups used in nucleophilic substitution reactions

copper(I) catalyzed radioiodination. Limitations of such a reaction are the harsh acidic conditions required for the formation of the diazonium salt and the potentially explosive diazonium salts. A one-pot radioiodination was reported where the diazonium salts were formed under mild reaction conditions. This was achieved using a polymer-supported nitrite reagent and *p*-toluene-sulphonic acid as a proton source, followed by the direct radioiodination. The solid phase support allows for simple and rapid purification [24].

Substitution of an iodine substituent with radioiodine is called homo/isotopic exchange whereas that of a bromine substituent is called hetero/halogen exchange. These reactions are typically referred to as radioiododehalogenation. Even though commonly used, the isotopic exchange suffers from low molar activity since the parent molecule cannot be separated from the product. When a bromine is being substituted with radioiodine the product can often be separated using chromatographic methods leading to higher specific activity. Ammonium sulphate facilitates solid-phase exchange radioiodination of unactivated aryl iodide. The process involves heating to partial decomposition of the salt to lower pH from 6 to 3 which is essential for the reaction as shown in Fig. 14.

Copper(I) catalyzes nucleophilic reactions by forming a 3-membered intermediate complex. Typically the Cu(I) is produced in situ by the reduction of Cu(II) by stannous chloride. The pH is maintained acidic to prevent nucleophilic attack by hydroxyl anions. The nucleophilic reaction can be also performed on boronated compounds as shown in Fig. 15. Higher radiochemical yields were obtained than electrophilic iododeborylation for compounds containing both electron-donating and electron-withdrawing substituents.

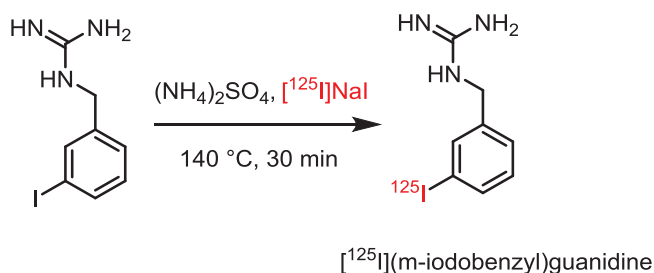


Fig. 14 Nucleophilic exchange reaction for the synthesis of $[^{125}\text{I}](m\text{-iodobenzyl})\text{guanidine}$

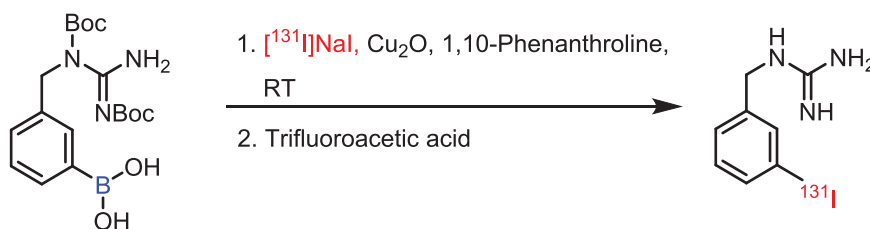


Fig. 15 Copper(I) catalyzed nucleophilic radioiodination of boronated compounds

3.3 Radiolabeling with Positron-Emitting Radionuclides

The most important positron emitters for radiolabeling of therapeutic nanosystems for diagnostics purposes are ^{18}F , ^{124}I , ^{64}Cu , and ^{89}Zr . All these radionuclides have sufficiently long half-lives for the radiolabeling of theranostic nanosystems, which typically have high molecular mass and slow pharmacokinetics (Table 3). From these nuclides, ^{18}F has the most optimal imaging characteristics, but also the shortest half-life ($t_{1/2} = 109.7$ min). Therefore, it can be used for tracing nanosystems with faster pharmacokinetics or by adapting a pretargeted radiolabeling strategy. ^{18}F does not have any theranostic nuclide pair, but nevertheless is an excellent choice as a diagnostic radionuclide when tracing therapeutic drug delivery systems, for example, for cancer chemotherapy. ^{124}I , ^{64}Cu , and ^{89}Zr have their theranostic pairs as ^{131}I , ^{67}Cu , and ^{90}Y respectively, which are all β^- emitters and widely used as radiotherapeutic agents in anticancer therapies.

The stability of the radiolabeling position is of utmost importance for both the diagnostic and therapeutic use of the nanosystem. Detached radionuclide may hamper the diagnostic use of a theranostic system, as the nuclear imaging will not be able to make any difference between different radioactive species. Especially if the detached radionuclide is bound to plasma proteins it may be difficult to differentiate whether the signal in circulation or tumor is originating from the protein-bound free radionuclide or from the radiolabeled theranostic nanosystem itself. For the radiotherapeutic use, the radiolabel instability is even more serious because the detached therapeutic radioisotope may cause serious adverse

Table 3 Positron emitting diagnostic radionuclides for theranostic systems

Radionuclide	Decay mode	Half-life ($t_{1/2}$)	$E_{\text{mean}} \beta^+$ in MeV (%)	Theranostic pair
^{18}F	β^+	109.7 m	0.250 (98)	None
^{64}Cu	β^+ , β^-	12.7 h	0.278 (9)	^{67}Cu
^{89}Zr	β^+	78.4 h	0.395 (13)	^{90}Y
^{124}I	β^+	4.18 d	0.687 (12)	^{131}I

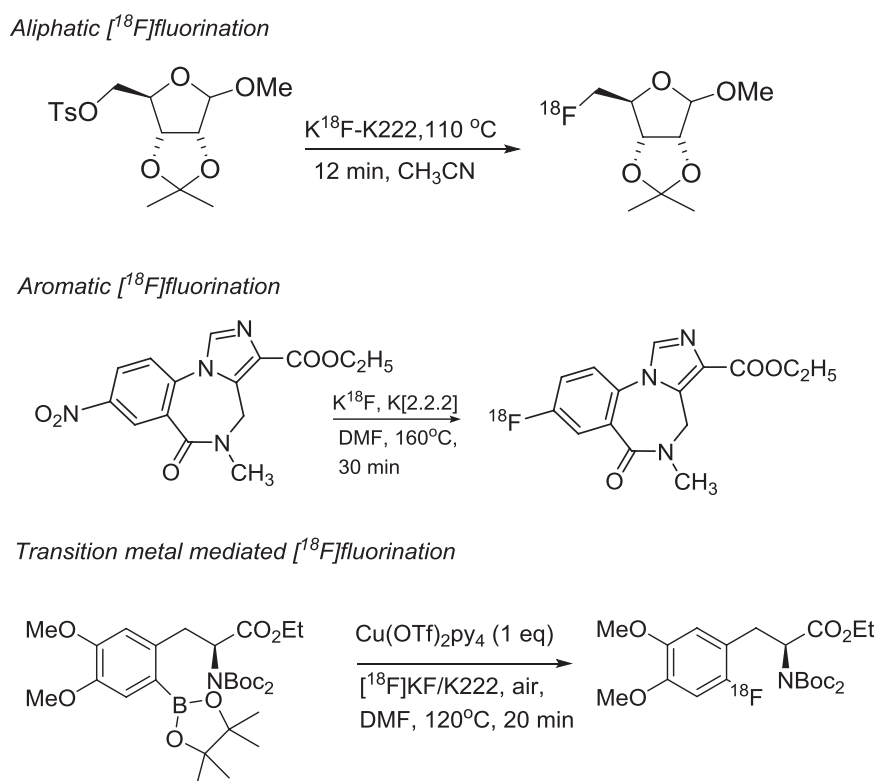


Fig. 16 Typical reaction conditions for [¹⁸F]fluorination

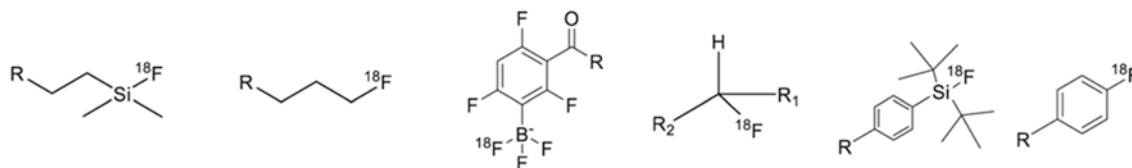
effects in radiation-sensitive healthy tissues such as the bone marrow, kidneys, and the intestinal epithelium. When using a true theranostic nuclide pair with different isotopes of the same element, the diagnostic and therapeutic nuclides exhibit identical chemical and pharmacokinetic properties and therefore the diagnostic system is perfectly suited for reliable evaluation of stability and biodistribution of the therapeutic system. In contrast, when radionuclides with different chemical properties are used, such as in case of ⁸⁹Zr/⁹⁰Y, more careful validation of the diagnostic accuracy of the system needs to be carried out before therapeutic use.

In principle, the chemical toolbox available for the radiolabeling of nanosystems is the same as in synthetic chemistry with stable isotopes. The only limitations for the use of short living radionuclides are the time available for the radiosynthesis and characterization, and the limited selection of the radioactive starting materials depending on production method of the selected radioisotope. The radioisotope production determines the chemical species of the produced radioisotope and the solvent or carrier gas in which they are delivered.

Fluorine can form stable covalent bonds with carbon and certain heteroatoms, such as silicon and boron. The formation of the carbon-[¹⁸F]fluorine bond is the most difficult to attain and anhydrous reaction conditions and high temperatures are needed in order to achieve high radiochemical yields, even with reactions mediated by transition metals (Fig. 16). In all cases, the stability of the bond is influenced by the groups adjacent to the [¹⁸F]fluorine. As fluorine is the most electronegative element in

the periodic table, it forms bonds which are strong, but highly polarized and can therefore be hydrolyzed by a nucleophilic attack. This can be overcome if the fluorine is stabilized by functional groups that can inductively compensate the positive partial charge of the fluorine binding atom and/or can sterically hinder it against the attack. The most stable carbon-[¹⁸F]fluorine bonds are between fluorine and an aromatic sp²-carbon, in which the delocalization of the partial positive charge to the aromatic ring can compensate for the bond polarization and decrease vulnerability of the bond against the nucleophilic attack. When fluorine is bound to a sp³-carbon, there is an additional mechanism which can lead to defluorination of the compound; in favorable conditions [¹⁸F]fluorine can be eliminated together with an adjacent proton (Fig. 17). Silicon is one of the least electronegative compounds and predominantly forms bonds as sp³-hybridized silicon. Polarization of the fluorine bond is most prominent for silicon and careful structure optimization is required in order to achieve stable [¹⁸F]fluorination to silicon. In addition to carbon, silicon, and boron, fluorine can form stable coordination complexes together with aluminum by generating an [¹⁸F]AlF²⁺ complex, which can be chelated analogously to several radiometals.

The radiolabeling methods for iodine-124 are described in Sect. 3.2. Only the radioiodination to sp²-carbon is stable in vivo. Radioiodination to a saturated position leads to quick elimination of the radiolabel and accumulation of the free iodine into the thyroid. The detachment of an iodine label can never be completely avoided, but accumulation into thy-



Increasing stability

Fig. 17 The bond type and the position influences stability against defluorination

roid can be minimized by pretreating the thyroid with iodine salts. Copper-64 and zirconium-89 are radiometals and can be incorporated to the nanosystems by chelation chemistry. As described already in Sect. 3.1., copper-64 exists predominantly in oxidation state II and its coordination number varies between 4 and 6. When using copper-64 for radiolabeling of nanotheranostics systems, it is especially important to notice its susceptibility to bind to endogenous proteins, such as ceruloplasmin and superoxide dismutase. The protein binding competes with binding to a chelator and may cause transchelation of the radiolabel from the nanostructure to the protein. Zirconium-89 is an emerging radionuclide in radiolabeling of nanosystems, due to its long half-life and low positron energy. The main challenge with zirconium-89 is stable chelation – all the existing chelators for $^{89}\text{Zr}^{4+}$ have exhibited limited *in vivo* stability leading to bone accumulation of the detached radiometal over time.

3.4 Pretargeted Radiolabeling Strategies

Instead of using direct labeling of nanosystems prior to their administration it is possible to utilize pretargeted radiolabeling strategies. In a pretargeted strategy, nanosystems are radiolabeled *in vivo* by using radiotracers which specifically bind to the administered nanosystem either by weak interactions or covalent bonds. One of the most investigated strategies for pretargeted radiolabeling is the biotin-(strept)avidin system, in which the recognition is based on the high-affinity interaction between biotin and avidin [25]. Other investigated pretargeted systems are, for example, systems based on hapten-antibody and DNA-DNA interactions [26, 27]. Recently, pretargeted strategies based on bioorthogonal chemical reactions have been under intensive investigation.

In *bioorthogonal* pretargeted strategies, the recognition between the tracer and a nanosystem is based on a chemical reaction, which leads to the formation of a covalent bond. Notably, the bioorthogonal reactions take place rapidly in physiological media without influencing the biological system. Several reactions have been investigated for the purpose

such as Staudinger ligation, strain-promoted cycloadditions and inverse electron-demand Diels-Alder cycloaddition (IEDDA). From these only the IEDDA reaction has been shown to exhibit fast enough kinetics in physiological conditions for use in living animals. In the IEDDA reaction, a cycloaddition product is formed between two functional groups, namely a tetrazine and a strained alkene such as trans-cyclooctene (TCO) (Fig. 18). Typically, a radiolabeled tetrazine is used for radiolabeling of a TCO-conjugated nanosystem due to the improved metabolic stability of functionalized tetrazines. Pretargeted PET imaging based on bioorthogonal chemical reactions has demonstrated great potential in nanotheranostic applications and may allow for the use of short-living radionuclides for tracing long-circulating nanosystems without unnecessary radiation exposure to the patient.

3.5 Radiolabeling with Alpha Emitters

Alpha emitters can be chelated to traditional chelators such as DOTA, but the recoil energy of the ^{225}Ac daughters after an α decay is so energetic that about 30% of the radioactivity is lost from the chelate. Radium-223 (^{223}Ra), lead-211 (^{211}Pb), francium-221 (^{221}Fr), and bismuth-211 (^{211}Bi) are the primary daughter isotopes and cause renal toxicity. ^{225}Ac and its daughter ions are oxophilic making it easy to bind to hydroxyl-rich surfaces such as that of titanium dioxide. To prevent the leaching of ions due to the alpha decay they have to be encapsulated in the nanosystem. TiO_2 nanoparticles were functionalized with peptide fragments targeted to glioma cells with PEG spacer. ^{225}Ac was incorporated by ion exchange on the hydroxyl groups. After 10 days of incubation in physiological buffer, 95% of ^{225}Ac and ^{221}Fr were retained in the nanoparticle core [29]. This type of exchange reactions can also be carried out on nanozeolites. Although produced chemically, nanozeolites have been shown to have low toxicity similar to silicon nanoparticles. ^{223}Ra labeled nanozeolites showed 90% retention after 6 days with up to 5% release of ^{211}Pb and ^{211}Bi [30]. Medically relevant

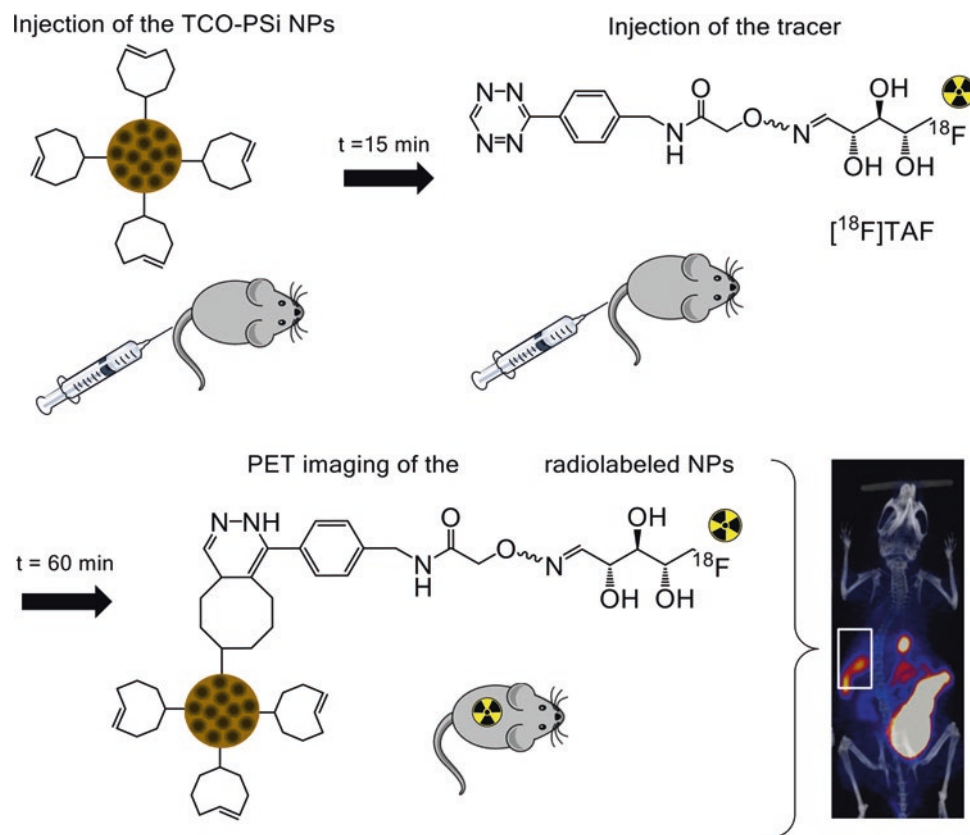


Fig. 18 Pretargeted PET imaging of a TCO-conjugated porous silicon nanosystem (TCO-PSi) in mice. The TCO-PSis were injected 15 minutes before injection of a ^{18}F -labeled tracer, $[^{18}\text{F}]\text{TAF}$. PET imaging was performed 60 minutes after injection of the tracer and the TCO-PSis were successfully traced in spleen (delineated by a box). Some accumulation also in liver was observed. The observed high levels of radioactivity in gall bladder, intestines and urinary bladder are caused by elimination of $[^{18}\text{F}]\text{TAF}$ and its radioactive metabolites. (Figure reprinted with permission from the American Chemical Society from reference [28])

poly(butadiene-*b*-ethylene oxide) was used to make liposomal vesicles. ^{225}Ac was chelated with ionophores such as calimycin and then incorporated into the liposomes. Recoil-ejected ^{213}Bi and ^{221}Fr could be separated from the unbound liposomes using DOWEX ion exchange resin and were found to be 47% and 31%, respectively [31].

Astatine-211 (^{211}At) is another promising alpha emitter belonging to the halogen series. As for iodine, prosthetic groups such as succinimidyl astatobenzoate (SAB) can be used to functionalize biomolecules. SAB is synthesized from a stannyl precursor using electrophilic halodemetalation reaction with an oxidant as shown in Fig. 19. The limitation of using oxidizing conditions is the multiple oxidation states available for astatine, which leads to low reproducibility and hence limits clinical application. With this respect, At^- is much easier to stabilize and hence nucleophilic reaction conditions are preferable. Nucleophilic substitution of arylodonium salt containing prosthetic groups using At^- (Fig. 20) was shown to have high radiochemical yields. The aryl group on the arylodonium salt which should not be radioastatinated was chosen to be electron rich to prevent attack of At^- . The *p*-anisyl group achieved the best radiochemical yields for radioastatination among *p*-isopropoxyphenyl and 2-thienyl groups [32].

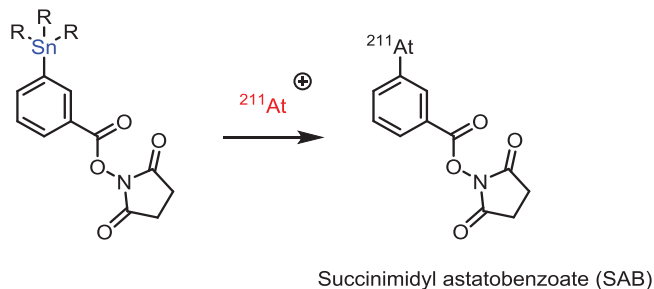


Fig. 19 Synthesis of prosthetic group containing Astatine-211

4 Preclinical Studies with Radiolabeled Tracers

Here, we give an overview of the standard preclinical *in vitro*, *ex vivo*, and *in vivo* methods employed in the biological evaluation of radiolabeled tracers including theranostic nanosystems. The focus is on methods where the output will be a measurement of the amount of radioactivity or visualization of its biodistribution. Conventional therapeutic efficacy and survival studies are to be used alongside to determine the therapeutic efficacy of the nanosystem.

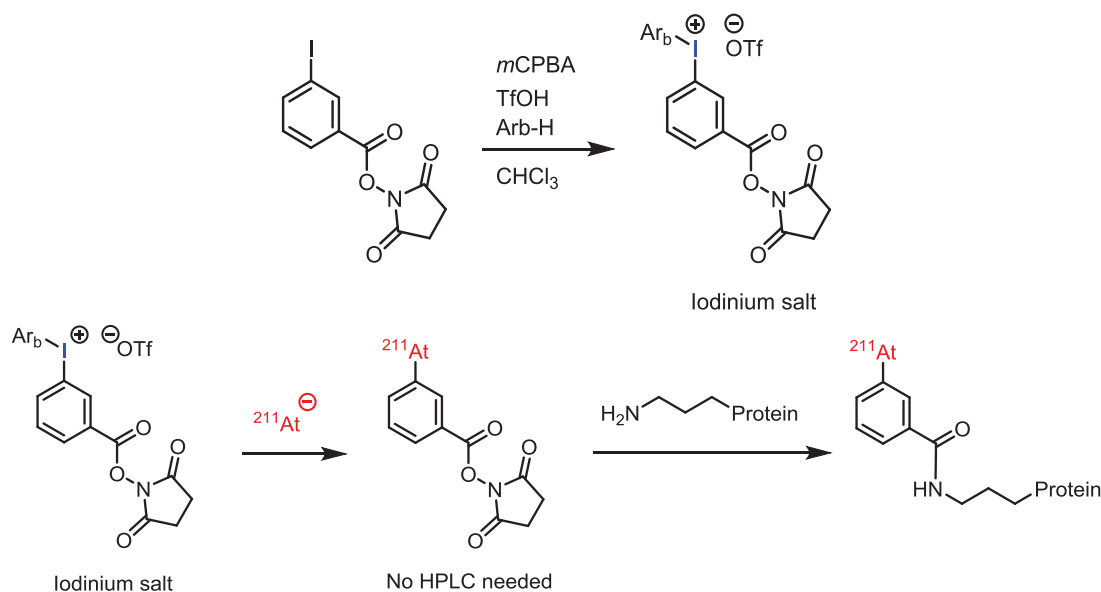


Fig. 20 Using iodine salts for nucleophilic substitution reactions

4.1 In Vitro Methods

The *in vitro* methods used in the evaluation of theranostic nanosystems include various radiolabel stability assays in physiologically relevant media and cell uptake studies for the determination of the nanosystem cellular interaction and internalization and to corroborate the specificity of the nanosystem targeting. Additionally, as a proof-of-concept, the therapeutic effects of theranostic nanosystems can be assessed *in vitro* using various cell viability assays, assays for reactive oxygen species (ROS) and inflammatory markers, as well as by immunofluorescence staining of cells for markers of radiation-induced DNA damage, apoptosis, senescence and by observing the radiation-induced synchronization of the cell cycle with flow cytometry [33].

4.1.1 Radiolabel Stability Assays

Since the chemical identity of a radioactive species cannot be readily identified from nuclear images or radioactivity measurements of excised tissues – in these the radioactive signal is related only to the radioisotope but not its chemical form – radiolabel stability needs to be rigorously evaluated *in vitro* before proceeding to *in vivo* studies. Typically, the radiolabeled tracer is incubated in physiological media relevant for the administration route (plasma, serum, simulated gastric or intestinal fluids, simulated lung fluid, or cell culture media) at 37°C over a period of time and samples are drawn from the incubations at designated time points and analyzed for the fraction of radioactivity remaining in the intact radiotracer. In the case of nanosystems, the nanoparticles are usually removed from the incubation by centrifugation or ultrafiltration and the amount of radioactivity remaining in

the collected nanoparticles and in the solution is measured. Alternatively, analytical methods such as size-exclusion chromatography (SEC) thin layer chromatography (TLC) with radioactivity detection can be used to more closely monitor for the presence of the intact radiolabeled nanoparticles and the free radiolabel. In this case, the analytical method needs to be set up so that the retention times for the two are sufficiently different and that a clear separation is obtained. Additionally, the level of radioactivity at the sample needs to be set up to a level that can provide a clear signal even after long incubations. The radiolabel stability should be followed for a duration of time meaningful for the *in vivo* application and for as long as reasonably permitted by the half-life of the radioisotope. If the theranostic nanosystem is intended for radiotherapy, for example, the stability should be followed for days, for an imaging study with a shorter-lived radioisotope a duration of few hours is often sufficient. The radiolabel stability should be exceeding 95% for the entire duration the stability assay.

4.1.2 Cell Uptake and Internalization Assays

Radioactivity is a convenient tool also for the quantification of the cellular internalization and targeting of theranostic nanosystems. In these assays, the radiolabeled nanoparticles are incubated with the targeted tumor cell line, and at designated time points the amount of radioactivity remaining in the media, on cell surface and in the cell lysate is determined by radioactivity measurement of the fractions. The specificity of the cellular uptake can be studied by preventing the targeting using a large molar excess of a competing ligand or nanosystems modified with, for example, nontargeting control sequences. The time frame for the experiment depends

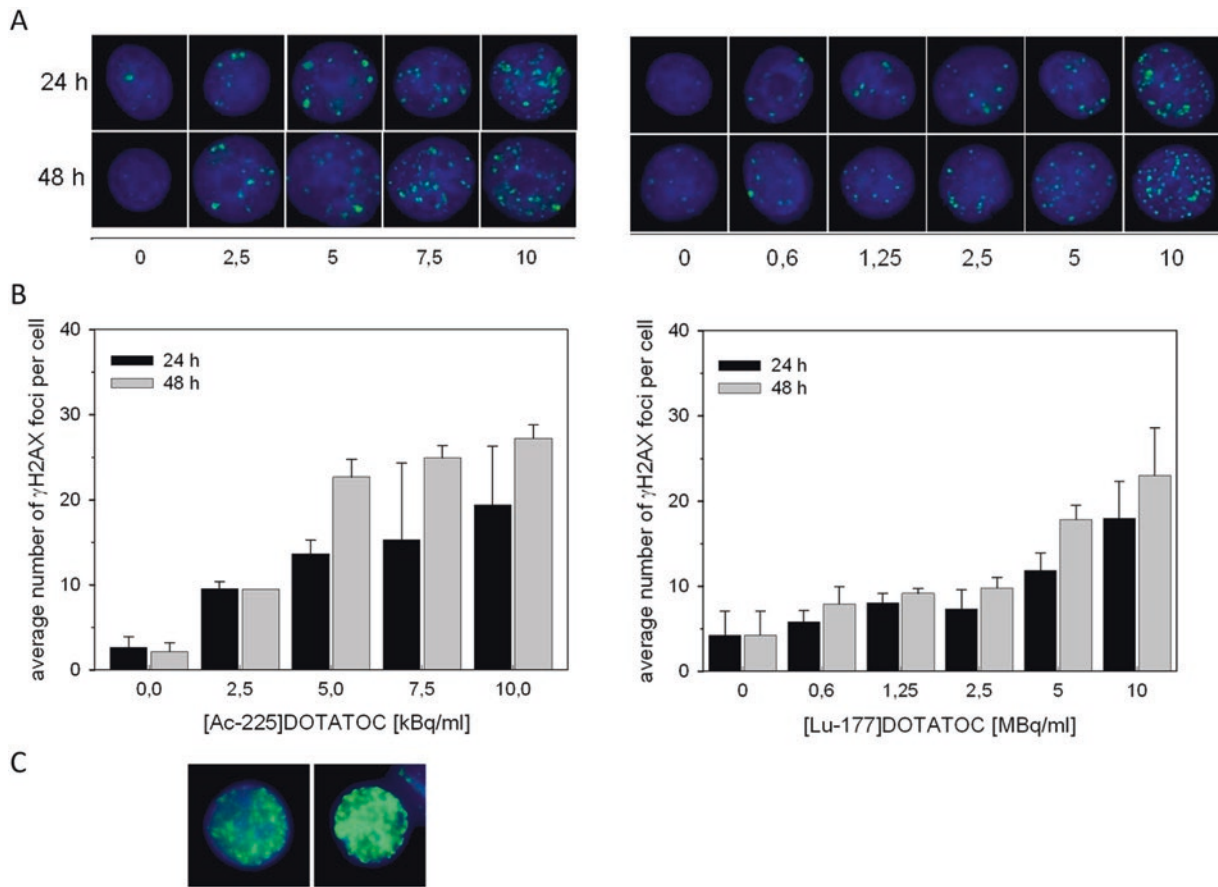


Fig. 21 Histone phosphorylation marker γ H2AX can be used to quantify the number of DNA double-strand breaks induced by radiation therapy. Number of γ H2AX foci in AR42J cells at 24 and 48 h after incubation with ^{225}Ac -DOTATOC (left) and ^{177}Lu -DOTATOC (right).

(a) shows representative images from all activity levels, (b) shows quantification of γ H2AX foci and (c) shows two representative examples for pan nuclear staining after high dose ^{225}Ac -DOTATOC treatment. (Figure reprinted with permission from reference [35])

on the system under study, but typically studies over a few hours or even 1–2 doubling times of the cell line can be done depending on the half-life of the radioisotope and its cytotoxicity.

4.1.3 Markers for Radiation-Induced Cellular Damage

Ionizing radiation induces a number of characteristic alterations in mammalian cells, and all of these can be used to determine the radiotherapeutic potential of the theranostic nanosystem. The DNA double-strand breaks induced by high LET α and β^- radiation can be visualized using γ H2AX, a marker of histone phosphorylation which occurs in response to the double-strand break [34]. γ H2AX has been shown to be a robust marker for radiation damage which is illustrated by the example in Fig. 21. The example from Graf and co-workers nicely illustrates by the number of γ H2AX foci in rat pancreatic adenocarcinoma cells the differences between the LET values for theranostic β^- emitter ^{177}Lu and the α emitter ^{225}Ac when delivered by the same vector, the somatostatin receptor targeting peptide DOTATOC [35].

Cells respond to the DNA damage elicited by ionizing radiation by the activation of two main pathways, one leading to apoptosis [36] and the other to premature aging, or senescence [37]. Staining for apoptosis using established markers such as TUNEL (terminal deoxynucleotidyl transferase dUTP nick-end labeling), active caspase-3, or Annexin V is widely used also in the context of radiotherapy to study cellular and tissue-level effects of radiation treatment. Entry into the premature senescence or senescence-associated secretory phenotypes (SASPs) can be studied using a number of hallmark markers for senescence, including senescence-associated β -galactosidase, decreased Ki67, and elevated trimethylated histone H3 lysine 9 (H3K9me3) [38, 39]. The DNA damage resulting from exposure to ionizing radiation activates checkpoint pathways that inhibit the progression of the cells through the G_1 and G_2 phases of the cell cycle and induce a transient delay in the progression through S phase. As a result, an arrest of cells in the G_2/M checkpoint can be seen. This can be studied, for example, by flow cytometry [33, 40].

4.2 Ex Vivo Biodistribution Studies and Autoradiography

The distribution of radiolabeled tracers in the body is in the preclinical setting most commonly determined in an ex vivo biodistribution study, where groups of animals ($n = 3-5$) are sacrificed at predetermined time points after administration and tissue samples are collected to pre-weighed tubes and measured on an automated gamma counter with weighed (approximately 10 μ l) standards prepared from the formulated radiotracer solution. The output in biodistribution studies is the percentage of the injected (radioactive) dose per gram of tissue (%ID/g). The injected dose is determined using the standards when the weight of the administered formulation is known (from weighing the syringe before and after administration). Depending on the application, the ex vivo biodistribution studies can be preceded by or conducted alongside small animal PET or SPECT/CT imaging studies discussed next.

Autoradiography is a sensitive imaging technique to study the tissue-level distribution of radiolabeled tracers ex vivo in cryosections prepared from tissue samples. The autoradiographic image can then be overlaid to a histological or immunofluorescence staining image of the same or adjacent section to correlate the radioactivity accumulation, for example, with the presence of the target of the theranostic nanosystem or physiological change elicited by the nanosystem accumulation. Today, most autoradiographic systems employ digital imaging plates instead of conventional X-ray films to record the autoradiographic image. In the digital imaging plate, the energy emitted by the radioisotope is stored by a phosphor layer of europium-doped barium fluoroborate crystals and released through the excitation of the Eu^{2+} to unstable Eu^{3+} when the plate is scanned with a red (633 nm) laser resulting in emission of blue light (390 nm) as the Eu returns to the ground state from the areas of the plate that were exposed to radiation. The emission is called photostimulated luminescence (PSL) and the quantification is often carried out in units of PSL/ mm^2 . Also real-time autoradiographic systems, where the tissue sample is encased in a parallel ionization multiplier (PIM) chamber are available. In these systems, the signal is accumulated as true counts or count rate per area, and the measurement time can be increased accordingly during the acquisition to improve the signal-to-background ratio in the image. In contrast, in digital autoradiography the autoradiographic trace is lost from the plate during the readout and in the case of short-lived isotopes only a single exposure will be possible.

4.3 Small Animal PET and SPECT/CT Imaging Studies

Small animal PET and SPECT/CT imaging technology allows for the noninvasive imaging of radiotracer biodistribution in laboratory rodents. Imaging studies are typically

conducted under inhalation anesthesia, and the commercial imaging systems contain solutions for the administration of anesthesia, warming the animals during the scan and nowadays also platforms for the imaging of multiple animals in a single scan. The power of imaging over the conventional ex vivo biodistribution studies described above is that the entire biodistribution – including organs that are not necessarily sampled for the gamma counting – can be seen in the image and thus possible unexpected accumulation will not go undetected. Furthermore, an individual animal can be followed up longitudinally using imaging, which reduces the number of animals needed for a study as well as allows for the account of inter-individual differences such as tumor heterogeneity or stage and disease progression on the study outcome. The ex vivo biodistribution studies are, however, usually needed at some point of radiotracer development to validate the results of the imaging and to provide quantification for images acquired with SPECT, a semiquantitative method. Imaging can be carried out through a *dynamic* acquisition protocol, where the imaging acquisition is started at the time of the radiotracer injection or immediately after to track the early passage of the radiotracer with sequentially acquired images typically over the first 60 minutes of injection. In *static* acquisition, the signal is collected over a fixed period of time or up to a desired number of counts giving a summed image of the radiotracer distribution. Most small animal imaging systems available today are hybrid systems, where an anatomical imaging modality such as CT or MRI is provided together with the nuclear imaging and workflows can be programmed for the sequential acquisition of the two.

4.4 Radiotherapy Studies and Dosimetry

The radiotherapeutic effects of theranostic nanosystems are most commonly determined by following the tumor size and attainment of the experiment humane endpoints after the administration of the radiotherapy. This can be done by conventional caliper measurements for subcutaneous or superficial orthotopic tumors, or, for example, by optical imaging of orthotopic tumors if a luciferase or fluorescent protein-expressing cell line is used, by regular weighing of the animals, and by the use of a technique called body condition scoring [41] to monitor the condition of the animals. In addition, the effects of the radiation exposure on the blood values (such as red blood cell count, hematocrit, white blood cell and platelet counts) of the animals are commonly studied as an indicator for hematological toxicity and when comparing different dosing regimens [42]. Dedicated veterinary systems for blood analysis in the small volumes collected from laboratory rodents are available. Another important factor for the feasibility of the clinical translation of a theranostic nanosystem will be the dosimetry, that is, the radioactive dose imparted by the nanosystem on the tumor and healthy tissues in the body. The dosimetry calculations are determined by

measuring the time activity curves (TAC) for the clearance of the radiotracer in selected organs (the %ID/g in each can be determined either by imaging or ex vivo biodistribution) and fitting a typically one or two-phase decay equation in the data. The area under the curve then gives the cumulative uptake which can be converted to the absorbed dose making the necessary assumptions for the absorbed fraction of the radiation and equilibrium absorbed dose constants depending on properties of the radioisotope. Human dosimetry for the same radiotracer can be extrapolated from the mouse data using a number of computational models and reference values such as those set forth by the International Commission for Radiation Protection (ICRP) [42–44].

5 Current Examples of Radiolabeled Theranostic Nanosystems

The nanostructured core of the theranostic nanosystems can be metallic, polymeric, or lipid based such as micelles and liposomes. The surface of the nanosystem is modified to make it biocompatible and functionalized for the conjugation of biological targeting agents, radiolabels, or therapeutic molecules. The surface modifications allow for the extension of the circulation half-life, the tailoring of pharmacokinetics (PK) and biodistribution (BD), the suppression of immunogenicity and antigenicity, the stabilization against enzymatic degradation, reduced efflux of drugs, improved cellular endocytosis, and change in solubility characteristics. Multimodal imaging is often used since the resolution and sensitivity of detection varies across modalities, and different capabilities are needed for addressing phenomena at different levels of organization [45]. The combinations of imaging modalities for multimodal imaging are chosen such that ideally anatomical, physiological and

molecular information is acquired with high sensitivity as illustrated by Fig. 22.

While passive targeting is more suited for fast growing tumors and nanoparticles which have a long circulation time, most tumors have unpredictable extravasation of the nanoparticle with varied sizes, shapes, and surface charge. Hence, targeting groups allow specific targeting beyond the effects of enhanced permeating and retention (EPR). This is particularly important in poorly vascularized small metastasis which are below 100 mm³ [46–48].

Therapeutic agents loaded onto the nanoparticle can be released passively or with the stimuli of light or tumor micro-environment. In certain types of therapy, the external stimuli directly modulate the therapy such as in laser assisted ablation therapy. Well known examples of such therapies are photodynamic therapy (PDT) and photothermal therapy (PTT) where the light stimuli activate the photosensitizer which could be a small molecule or a nanoparticle. The imaging techniques that have been used are PET, SPECT, CT, MRI, optical/photoacoustic imaging, and contrast enhanced ultrasound [49, 50].

Diagnostic and therapeutic radioisotopes such as copper-64 and lutetium-177 can be bound to the same DOTA chelator. They have been loaded onto DOTA containing liposomes and used for PET imaging and therapy. Using PET imaging the optimum PEGylation and its influence on the biodistribution and tumor accumulation can be determined. A high therapeutic dose (114 mGy/MBq) could be delivered to the tumor site for the lutetium-177 loaded liposomes [51]. Liposomal formulations using doxorubicin as a chemotherapeutic agent in combination with rhenium-188 which has therapeutic properties as well SPECT imaging capabilities have been shown to greatly inhibit tumor growth and enhance the median survival time in a murine colon carcinoma model. The therapeutic results were better than singly functional-

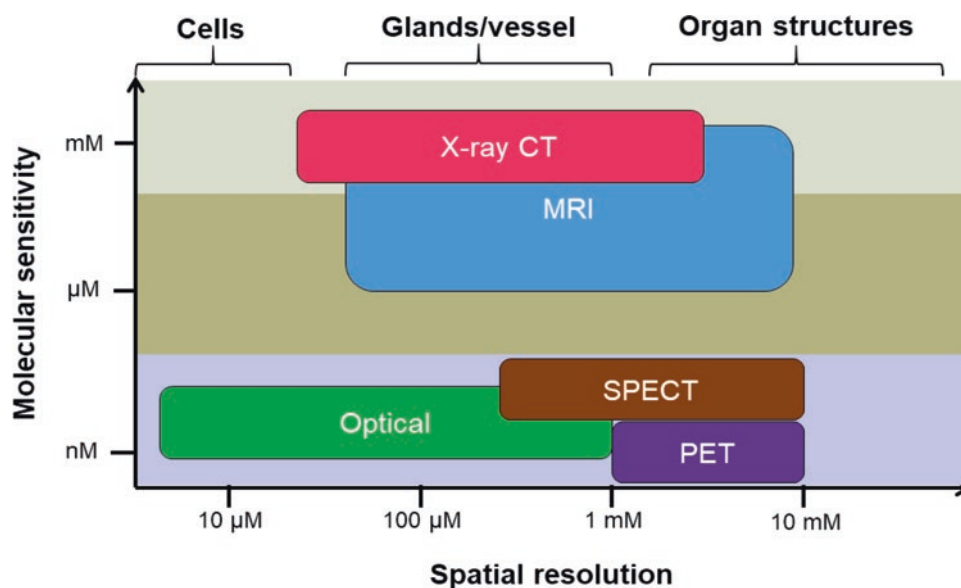


Fig. 22 Precision and sensitivity of detection varies across imaging modalities

ized rhenium-188-liposomes or doxorubicin-liposomes which shows that the synergistic effects of chemotherapy and internal radiation therapy are far more effective in therapy [52]. Multifunctional liposomes have been reported which have been loaded with doxorubicin for therapy, gadolinium ions for MR imaging, IRDye for NIR fluorescence imaging, technetium-99m for SPECT imaging, and copper-64 for PET imaging. In these dipalmitoyl phosphatidylcholine (DSPC)-based liposomes, the drug was encapsulated, technetium-99m was post loaded, while the copper-64 was conjugated to the DOTA chelators available on the liposome surface. The liposomes showed effective and correlated multimodal imaging capabilities in a murine model of head and neck cancer [53]. The drug delivery and therapeutic response was quantified in a clinical study with copper-64 labeled HER2 targeted PEGylated liposomal doxorubicin (Doxil). This study provided evidence that the EPR effect is functional in human tumor and imaging liposomal deposition can identify patients who are ideal for receiving therapeutic liposomes. The concentration, rates of deposition, and washout of the liposomes in human tumor are comparable to preclinical models, which is of high significance for future studies [54]. Such image-guided insights are useful to prescreen patients assigned to Doxil in order to identify which patients are likely to respond to therapy and which are not. The release of a doxorubicin from liposomes could be visualized using MRI by using MR contrast agents such as manganese ions which were mixed with doxorubicin and upon simultaneous liberation enhanced contrast due to increase in water exchange rates. Other studies with MRI contrast agents to follow drug release have used ProHance (Gd-HP-DO3A) [55, 56]. Alpha particles have short penetration depth and high linear energy transfer (LET) which gives them an advantage over beta or gamma radiation. Alpha particle emitters such as ^{225}Ac , ^{223}Ra and ^{224}Ra have made it to the clinic. The limitations associated with alpha emitters are that the daughter ions when not retained at the tumor site can cause significant damage to healthy tissue. ^{211}Bi causes renal toxicity which is a limiting factor for performing clinical studies. The ^{225}Ac could be doped into the core of a nanoparticle prepared from lanthanum chloride, gadolinium chloride and cross-linked with sodium tripolyphosphate. The core nanoparticle is then covered with layers of gadolinium phosphate and gold. The magnetic properties of gadolinium phosphate allow easy separation and the gold surface provides biocompatibility and easy attachment of targeting moieties. The multilayered structure allowed 99.9% retention of ^{225}Ac and 98% retention of daughter ions. The gamma rays from the ^{221}Fr allow SPECT/CT imaging. The nanoparticles with antibodies targeted to the thrombomodulin receptors of lung showed predominant lung uptake 1 h post injection [57].

Carbon-based nanomaterials include fullerenes, carbon nanotubes, graphenes, and carbon-based quantum dots. The

intrinsic property of one-photon and two-photon fluorescence in the NIR II allows deep tissue optical imaging. Their biocompatibility and ease of functionalization make them interesting candidates for theranostic applications. A ^{64}Cu labeled doxorubicin loaded polydopamine-gadolinium-metallofullerene ($\text{Gd}_3\text{N@C}_{80}$) core-satellite nanotheranostics was prepared which was capable of MR/photoacoustic/PET imaging and NIR triggered drug delivery in combination with PTT. The gadolinium showed high T1 contrast and was retained well in the particles. The doxorubicin was bound to the polydopamine through π - π stacking and hydrogen-bonding interactions, which were disrupted with NIR, causing the release of doxorubicin. The PTT caused the tumor temperature to reach 46 °C with 808 nm laser in 10 min and the combination therapy slowed the tumor growth and was significantly more effective than the monotherapy [58]. Single wall carbon nanotube (SWCNT) have inherent Raman signature which allows the direct monitoring of the presence of nanotubes in mice tissue. They were covalently attached to DOTA or DFO to chelate to actinium-225 or zirconium-89, respectively. The SWCNT was attached to tumor neovascular-targeting antibody E4G10. The alpha particles from ^{225}Ac have a travelling distance which match the vessel dimensions and delivers high linear energy transfer (LET) to the cells resulting in acute cytotoxicity making it ideal vascular-targeted radioimmunotherapy. The ^{89}Zr labeled constructs allowed PET imaging and determination of pharmacokinetics of the construct [59]. PET imaging and dosimetry of ^{90}Y SIR-Sphere using ^{86}Y and ^{89}Zr radiolabeled surrogates could be performed, and showed in vivo stability for clinical application. Theranostic application could be easily envisioned with the similarity in half lives of ^{89}Zr and ^{90}Y [60].

Gold nanoparticles can be prepared in different geometries, such as nanospheres, nanoshells, nanorods, or nanocages, which along with size affect the photothermal conversion efficiency for photothermal therapy. The absorbed wavelength changes depending on the shape of the particle so it has to be tuned such that it absorbs NIR in the two biologically transparent optical windows available, 650–850 nm and 950–1350 nm. The gold surface is ideal for binding to free thiol which makes it an ideal choice for bioconjugation. Copper sulphide nanoparticles are advantageous to gold nanoparticles as they are considered biodegradable inorganic nanomaterials, the surrounding environment does not affect its absorption wavelength and lastly, the cost of production is much lower. CuS nanoparticles were coupled to ^{64}Cu using chelator-free methods and used for PTT therapy with 800 and 980 nm laser showing better photothermal effects with 980 nm laser. The photothermal conversion efficiencies of the CuS nanoparticles were reported to be much higher than gold nanospheres and SWCNTs with 980 nm laser reaching 99.85 °C at 2 W/cm²

for 4 min. The biodistribution of the particles was assessed using PET imaging and image guided PTT could be performed with a thermal mapping system equipped with an MRI scanner. In the orthotopic ovarian cancer mice model, this resulted in an effective therapeutic outcome [61]. To improve on the previous results in terms of the tumor availability of the nanoparticle, RGDfK peptides were attached to the CuS nanoparticles to target the $\alpha\text{v}\beta\text{3}$ integrins and labeled with ^{64}Cu in a chelator-free fashion as before. For the therapy a lower wavelength of 808 nm at 3 W/cm² for 2 min was used which increased the tumor temperature to 58.1 °C and resulted in 98% tumor tissue necrosis in U87 tumor-bearing mice [62]. Similar constructs can be used to target other biomarkers such as folate receptors, which are overexpressed in ovarian, breast, lung, and head and neck cancers [63]. CuS nanoparticles were loaded in PLGA microspheres together with the chemotherapeutic paclitaxel and radiolabeled with ^{131}I . These were used for PTT, chemotherapy, radiotherapy, photoacoustic imaging, and SPECT/CT from a single construct. The trimodal combination therapy with NIR irradiation eliminated tumor growth after intratumoral injection at relatively low doses in the orthotopic breast cancer model [64]. Theranostic Gd:CuS@BSA nanoparticles were prepared using copper(II) sulphide and gadolinium(III) ions with bovine serum albumin (BSA) as a scaffold. The 9 nm particles showed high photothermal conversion efficiency and good photostability under near-infrared (NIR) laser irradiation. Mice with ovarian cancer xenograft showed tumor growth inhibition with 5 min irradiation using 980 nm laser irradiation with the tumor temperature going up to 50 °C [65]. Defect-rich multifunctional Cu-doped layered double hydroxide (Cu-LDH) nanoparticles were shown to have pH enhanced NIR PTT as well as pH-sensitive T1 weighted MRI properties. The peculiar microstructures gave these nanoparticles high photothermal conversion at 808 nm and pH sensitivity. Further these particles were loaded with the chemotherapeutic agent 5-FU to combine PTT with chemotherapy and dose-dependent cytotoxicity was observed. Mice with colon cancer xenografts could be MR imaged and showed complete ablation with the combination of PTT and chemotherapy [66].

A melanin-based nanosystem with inherently good biocompatibility, biodegradability, and intrinsic photoacoustic properties was functionalized with tyrosine kinase inhibitor, sorafenib using π - π interaction. In addition, these particles had the natural ability to bind ^{64}Cu or ferric ions for PET or MR imaging studies. PET imaging allowed accurate and sensitive measurement of tissue penetration of the agent whereas the photoacoustic imaging allowed superficial information due to limitations of the penetrability of the NIR laser. Significant tumor shrinkage was observed from a single dose of the agent [67, 68].

Water-soluble superparamagnetic iron oxide (SPIO) nanoparticles such as ferumoxides and ferucarbotrans are clinically approved for MR imaging of the liver diseases. The approval of the SPIO makes them potential candidates for further approval as drug delivery candidates. PEGylated SPIOs were functionalized with cRGD for targeted tumor delivery. They were conjugated with ^{64}Cu using NOTA as chelators for PET imaging. The pH sensitive drug delivery was achieved using hydrazone linked doxorubicin which showed effective release at pH 5.3. Quantifying the PET images showed that targeting the SPIOs with cRGD resulted in doubling of nanoparticle delivery [69].

The drug release from the nanoparticle can be triggered by various external stimuli such as ultrasound, light, thermal, or chemical environment changes. The success of the PDT-based treatment is not without its drawbacks. Since the photosensitizers are always in an “ON” state, patients are typically vulnerable to sunlight even after 4–6 weeks of the PDT therapy. Additionally, the hypoxic conditions of the tumor microenvironment hinder PDT therapy due to its inherent requirement for oxygen to generate reactive oxygen species. A nanoparticle (PcS-MA) formed from the host-guest interactions of water-soluble photosensitizer, zinc(II) phthalocyanine tetrasubstituted with 6,8-disulfonate-2-naphthylloxy groups, and the common anticancer drug, mitoxantrone (MA) were quenched in supramolecular structure and showed no PDT effect or fluorescence signal. Upon interaction with nucleic acids, the construct disassembles resulting in PDT and chemotherapy, and could be imaged using fluorescence. MCF7 tumor-bearing mice which were injected with PcS-MA and irradiated with 1 W/cm² for 5 min reached a maximum temperature of 42.7 °C at the tumor site and was able to inhibit tumor growth. Thus, such an activatable theranostic strategy could circumvent the drawbacks of traditional PDT in clinical settings [66].

The onset of hypoxia from PDT has been used as a trigger for a hypoxia activated prodrug AQ4N. The liposomal system was prepared by encapsulating AQ4N and hexadecylamine conjugated Ce6 (hCe6) photosensitizer in PEGylated liposomes which had a size of 95 nm. Conjugating the hCe6 with a positron emitter such as ^{64}Cu allowed PET imaging along with the inherently available fluorescence and photoacoustic imaging. All three modalities allowed the visualization of the liposomal delivery in the breast cancer model in mice with PET being the most sensitive. Biodistribution studies with the PET tracer also allowed quantification of the delivered dose. The therapy regimen showed that the synergistic effects of PDT and the hypoxia driven drug activation resulted in stagnation of the tumor growth [70].

Delivery of the drug to the tumor site is a challenge due to the insufficient accumulation of the nanoparticle. The size of the nanoparticle has to be optimized to have the desired

blood circulation time. Other constraints which favor small particle size are inefficient tumor vascular extravasation, high interstitial fluid pressure, and dense extracellular matrix. Nanoparticles with smaller size are hence desired because of their high diffusion to the tumor tissue but a size less than 5 nm results in rapid excretion through the kidneys. Another crucial factor is the charge of the nanoparticles which should be preferably positive for improved cellular interaction and internalization. However, immune responses such as opsonization occur more readily on positively charged particles and speeding up the elimination from the bloodstream. Xue et al. developed upPhD theranostic nanovehicles, which had a dual size and charge transformability from the acidic pH of the tumor microenvironment. The monomers (PhD) were synthesized by conjugating cytotoxic doxorubicin and the PDT agent, pheophorbide using pH sensitive hydrazone bonds. The monomers first self-assembled into ultra-small micelles (upPhD) of about 4 nm in size. The upPhDs were then pegylated using pH sensitive imine bonds to form particles (pPhD) with 79 nm in size. When pPhDs were exposed to acidic pH, hydrolysis of the pegylation resulted in reverting to the smaller sized upPhD particles. The strong positive charge of upPhD (43 mV) was reduced to 12 mV upon the formation of the pegylated pPhD particles at neutral pH but reverted back to 35 mV at pH 6.8. The fluorescence of both the monomer components was also quenched in pPhD particles but was regained at a pH of 6.8. In subcutaneous and orthotropic tumor mice models, the pPhD particles showed 100% cure rate and outperformed the upPhD particles showing the importance of charge and size modulation. The large, slightly positive nanovehicles had a long circulation time but could be broken down into ultra-small nanoparticles with high positive charge near the tumor microenvironment, ideal for cell penetration. The particle accumulation at the tumor site could be followed using the fluorescence signal of the monomers as well as by MR imaging of manganese ions bound to the PDT agent [71].

Biomimetic design strategies such as the ones using cell-derived membranes to synthesize natural-mimicking vesicles are particularly interesting due to their excellent biocompatibility, low toxicity, high tumor accumulation, and ability to evade the immune and reticuloendothelial systems. Multicompartment membrane-derived liposomes (MCLs) have been prepared using 4T1 breast cancer cell membranes fused with surfactant, Tween-80, and had a size of 140 nm which was considerably smaller than without Tween-80. The quantitative biodistribution study using DFO conjugated ^{89}Zr showed greater than 9% ID/g in the 4T1 breast cancer tumor model in mice and clearance mostly through the liver. Injection to the lymphatic system allowed imaging of the lymph nodes. PDT agent loaded liposomes showed reduction in the rate of growth of the tumor upon irradiation with 660 nm laser [72].

6 Conclusion

In this chapter, we have outlined the primary ways of introducing therapeutic and diagnostic radioisotopes to theranostic nanosystems of variable compositions and illustrated the vast potential of using radioisotope methods to monitor the behavior of the nanosystems in vivo as well as to deliver efficient therapy. With this knowledge, we are hopeful that the reader is now equipped with an overview on how to go about designing radiolabeled theranostic nanosystems as well as the safe handling of radioisotopes and the principles of the analysis of data based on radioactivity. As we can see, the choice of the available radioisotopes, labeling chemistries, and nanomaterial scaffolds gives rise to an exceptionally wide array of radiolabeled constructs for different purposes. Furthermore, theranostic nanosystems are an ideal platform for the generation of multimodality imaging probes which can provide information on the nanosystem performance across imaging modalities and resolution barriers using the same imaging tracer.

References

1. Kang, H., Hu, S., Cho, M. H., Hong, S. H., Choi, Y., & Choi, H. S. (2018). Theranostic nanosystems for targeted cancer therapy. *Nano Today*, 23, 59–72.
2. Drude, N., Tienken, L., & Mottaghy, F. M. (2017). Theranostic and nanotheranostic probes in nuclear medicine. *Methods*, 130, 14–22.
3. Aghevlian, S., Boyle, A. J., & Reilly, R. M. (2017). Radioimmunotherapy of cancer with high linear energy transfer (LET) radiation delivered by radionuclides emitting α -particles or Auger electrons. *Advanced Drug Delivery Reviews*, 109, 102–118.
4. Ku, A., Facca, V. J., Cai, Z., & Reilly, R. M. (2019). Auger electrons for cancer therapy - a review. *EJNMMI Radiopharmacy and Chemistry*, 4, 27.
5. Eckelman, W. C., Boyd, M., & Mairs, R. J. (2017). Principles of molecular targeting for radionuclide therapy. In H. W. Strauss, G. Mariani, D. Volterrani, & S. M. Larson (Eds.), *Nuclear oncology: From pathophysiology to clinical applications* (pp. 35–65). Cham: Springer International Publishing.
6. Schirmacher, R., Wängler, B., Bailey, J., Bernard-Gauthier, V., Schirmacher, E., & Wängler, C. (2017). Small prosthetic groups in 18 F-radiochemistry: Useful auxiliaries for the design of 18 F-PET tracers. *Seminars in Nuclear Medicine*, 47, 474–492.
7. Coenen, H. H., Gee, A. D., Adam, M., Antoni, G., Cutler, C. S., Fujibayashi, Y., et al. (2017). Consensus nomenclature rules for radiopharmaceutical chemistry — Setting the record straight. *Nuclear Medicine and Biology*, 55, v–xi.
8. Bergström, M., Grahnén, A., & Långström, B. (2003). Positron emission tomography microdosing: A new concept with application in tracer and early clinical drug development. *European Journal of Clinical Pharmacology*, 59, 357–366.
9. Price, E. W., & Orvig, C. (2014). Matching chelators to radiometals for radiopharmaceuticals. *Chemical Society Reviews*, 43, 260–290.
10. Zhou, M., Chen, Y., Adachi, M., Wen, X., Erwin, B., Mawlawi, O., et al. (2015). Single agent nanoparticle for radiotherapy and radio-photothermal therapy in anaplastic thyroid cancer. *Biomaterials*, 57, 41–49.

11. Uccelli, L., Martini, P., Pasquali, M., & Boschi, A. (2017). Monoclonal antibodies radiolabeling with Rhenium-188 for Radioimmunotherapy. *BioMed Research International*, 2017, 5923609.
12. Yuan, H., Wilks, M. Q., El Fakhri, G., Normandin, M. D., Kaittanis, C., & Josephson, L. (2017). Heat-induced-radiolabeling and click chemistry: A powerful combination for generating multifunctional nanomaterials. *PLoS One*, 12, e0172722.
13. Boros, E., Bowen, A. M., Josephson, L., Vasdev, N., & Holland, J. P. (2015). Chelate-free metal ion binding and heat-induced radiolabeling of iron oxide nanoparticles. *Chemical Science*, 6, 225–236.
14. Hoffman, D., Sun, M., Yang, L., McDonagh, P. R., Corwin, F., Sundaresan, G., et al. (2014). Intrinsically radiolabelled [⁵⁹Fe]-SPIONs for dual MRI/radionuclide detection. *American Journal of Nuclear Medicine and Molecular Imaging*, 4, 548–560.
15. Shi, S., Fliss, B. C., Gu, Z., Zhu, Y., Hong, H., Valdovinos, H. F., et al. (2015). Chelator-free labeling of layered double hydroxide nanoparticles for in vivo PET imaging. *Scientific Reports*, 5, 16930.
16. Shi, S., Xu, C., Yang, K., Goel, S., Valdovinos, H. F., Luo, H., et al. (2017). Chelator-free radiolabeling of nanographene: Breaking the stereotype of chelation. *Angewandte Chemie (International Ed. in English)*, 56, 2889–2892.
17. Jakobsson, U., Mäkilä, E., Airaksinen, A. J., Alanen, O., Etilä, A., Köster, U., et al. (2019). Porous silicon as a platform for radiation theranostics together with a novel RIB-based radiolanthanoid. *Contrast Media & Molecular Imaging*, 2019, 3728563.
18. Kabalka, G. W., & Yao, M.-L. (2009). No-carrier-added radiohalogenations utilizing organoboranes: The synthesis of iodine-123 labeled curcumin. *Journal of Organometallic Chemistry*, 694, 1638–1641.
19. Ishiyama, T., Murata, M., & Miyaura, N. (1995). Palladium(0)-catalyzed cross-coupling reaction of Alkoxydiboron with Haloarenes: A direct procedure for arylboronic esters. *The Journal of Organic Chemistry*, 60, 7508–7510.
20. Hunter, R. (1970). Standardization of the chloramine-T method of protein iodination. *Experimental Biology and Medicine*, 133, 989–992.
21. Conlon, J. M. (1997). The use of IODO-GEN for preparing ¹²⁵I-labeled peptides and their purification by reversed-phase high performance liquid chromatography. *Methods in Molecular Biology*, 73, 231–237.
22. Krohn, K. A., Knight, L. C., Harwig, J. F., & Welch, M. J. (1977). Differences in the sites of iodination of proteins following four methods of radioiodination. *Biochimica et Biophysica Acta (BBA) - Protein Structure*, 490, 497–505.
23. Bolton, A. E., & Hunter, W. M. (1973). The labelling of proteins to high specific radioactivities by conjugation to a ¹²⁵I-containing acylating agent. Application to the radioimmunoassay. *Biochemical Journal*, 133, 529–538.
24. Sloan, N. L., Luthra, S. K., McRobbie, G., Pimlott, S. L., & Sutherland, A. (2017). A one-pot radioiodination of aryl amines via stable diazonium salts: Preparation of ¹²⁵I-imaging agents. *Chemical Communications*, 53, 11008–11011.
25. Cauchon, N., Langlois, R., Rousseau, J. A., Tessier, G., Cadorette, J., Lecomte, R., et al. (2007). PET imaging of apoptosis with ⁶⁴Cu-labeled streptavidin following pretargeting of phosphatidylserine with biotinylated annexin-V. *European Journal of Nuclear Medicine and Molecular Imaging*, 34, 247–258.
26. Honarvar, H., Westerlund, K., Altai, M., Sandström, M., Orlova, A., Tolmachev, V., et al. (2016). Feasibility of Affibody molecule-based PNA-mediated radionuclide pretargeting of malignant tumors. *Theranostics*, 6, 93–103.
27. van Rij, C. M., Frielink, C., Goldenberg, D. M., Sharkey, R. M., Franssen, G. M., Lütje, S., et al. (2014). Pretargeted ImmunoPET of prostate cancer with an anti-TROP-2 x anti-HSG bispecific antibody in Mice with PC3 Xenografts. *Molecular Imaging and Biology*, 17, 94–101.
28. Keinänen, O., Mäkilä, E. M., Lindgren, R., Virtanen, H., Liljenbäck, H., Oikonen, V., et al. (2017). Pretargeted PET imaging of trans-Cyclooctene-modified porous silicon nanoparticles. *ACS Omega*, 2, 62–69.
29. Cędrowska, E., Pruszyński, M., Majkowska-Pilip, A., Męczyńska-Wielgosz, S., Bruchertseifer, F., Morgenstern, A., et al. (2018). Functionalized TiO₂ nanoparticles labelled with ²²⁵Ac for targeted alpha radionuclide therapy. *Journal of Nanoparticle Research*, 20, 83.
30. Piotrowska, A., Męczyńska-Wielgosz, S., Majkowska-Pilip, A., Koźmiński, P., Wójciuk, G., Cędrowska, E., et al. (2017). Nanozeolite bioconjugates labeled with ²²³Ra for targeted alpha therapy. *Nuclear Medicine and Biology*, 47, 10–18.
31. Wang, G., de Kruijff, R. M., Rol, A., Thijssen, L., Mendes, E., Morgenstern, A., et al. (2014). Retention studies of recoiling daughter nuclides of ²²⁵Ac in polymer vesicles. *Applied Radiation and Isotopes*, 85, 45–53.
32. Guerard, F., Navarro, L., Lee, Y. S., Roumesy, A., Alliot, C., Cherel, M., et al. (2017). Bifunctional arylidonium salts for highly efficient radioiodination and astatination of antibodies. *Bioorganic & Medicinal Chemistry*, 25, 5975–5980.
33. Teiluf, K., Seidl, C., Blechert, B., Gaertner, F. C., Gilbertz, K.-P., Fernandez, V., et al. (2014). α-Radioimmunotherapy with ²¹³Bi-anti-CD38 immunoconjugates is effective in a mouse model of human multiple myeloma. *Oncotarget*, 6, 4692.
34. Kuo, L. J., & Yang, L.-X. (2008). γ-H2AX - A Novel Biomarker for DNA Double-strand Breaks. *In Vivo*, 22, 305–309.
35. Graf, F., Fahrner, J., Maus, S., Morgenstern, A., Bruchertseifer, F., Venkatachalam, S., et al. (2014). DNA double strand breaks as predictor of efficacy of the alpha-particle emitter Ac-225 and the electron emitter Lu-177 for somatostatin receptor targeted radiotherapy. *PLoS One*, 9, e88239.
36. Haimovitz-Friedman, A., Yang, T. J., Thin, T. H., & Verheij, M. (2012). Imaging radiotherapy-induced apoptosis. *Radiation Research*, 177, 467–482.
37. Wang, Y., Boerma, M., & Zhou, D. (2016). Ionizing radiation-induced endothelial cell senescence and cardiovascular diseases. *Radiation Research*, 186, 153–161.
38. Lee, S., & Schmitt, C. A. (2019). The dynamic nature of senescence in cancer. *Nature Cell Biology*, 21, 94–101.
39. Campisi, J., & d'Adda di Fagagna F. (2007). Cellular senescence: When bad things happen to good cells. *Nature Reviews Molecular Cell Biology*, 8, 729.
40. Iliakis, G., Wang, Y., Guan, J., & Wang, H. (2003). DNA damage checkpoint control in cells exposed to ionizing radiation. *Oncogene*, 22, 5834–5847.
41. Ullman-Cullere, M. H., & Foltz, C. J. (1999). Body condition scoring: A rapid and accurate method for assessing health status in mice. *Laboratory Animal Science*, 49, 319–324.
42. Poty, S., Carter, L. M., Mandleywala, K., Membreno, R., Abdel-Atti, D., Ragupathi, A., et al. (2019). Leveraging bioorthogonal click chemistry to improve ²²⁵Ac-radioimmunotherapy of pancreatic ductal adenocarcinoma. *Clinical Cancer Research*, 25, 868–880.
43. Keinänen, O., Brennan, J. M., Membreno, R., Fung, K., Gangangari, K., Days, E. J., et al. (2019). Dual radionuclide theranostic pretargeting. *Molecular Pharmaceutics*, 16, 4416–4421.
44. Stabin, M. G., & Siegel, J. A. (2003). Physical models and dose factors for use in internal dose assessment. *Health Physics*, 85, 294–310.
45. Gao, X., Guo, L., Li, J., Thu, H. E., & Hussain, Z. (2018). Nanomedicines guided nanoimaging probes and nanotherapeutics for early detection of lung cancer and abolishing pulmonary metas-

- tasis: Critical appraisal of newer developments and challenges to clinical transition. *Journal of Controlled Release*, 292, 29–57.
46. Maeda, H., Sawa, T., & Konno, T. (2001). Mechanism of tumor-targeted delivery of macromolecular drugs, including the EPR effect in solid tumor and clinical overview of the prototype polymeric drug SMANCS. *Journal of Controlled Release*, 74, 47–61.
 47. Allen, T. M. (2004). Drug delivery systems: Entering the mainstream. *Science*, 303, 1818–1822.
 48. Chen, F., Ehlerding, E. B., & Cai, W. (2014). Theranostic nanoparticles. *Journal of Nuclear Medicine*, 55, 1919–1922.
 49. Jokerst, J. V., & Gambhir, S. S. (2011). Molecular imaging with theranostic nanoparticles. *Accounts of Chemical Research*, 44, 1050–1060.
 50. Zavaleta, C., Ho, D., & Chung, E. J. (2018). Theranostic nanoparticles for tracking and monitoring disease state. *SLAS Technology*, 23, 281–293.
 51. Petersen, A. L., Henriksen, J. R., Binderup, T., Elema, D. R., Rasmussen, P. H., Hag, A. M., et al. (2015). In vivo evaluation of PEGylated 64Cu-liposomes with theranostic and radiotherapeutic potential using micro PET/CT. *European Journal of Nuclear Medicine and Molecular Imaging*, 43, 941–952.
 52. Chang, Y.-J., Chang, C.-H., Yu, C.-Y., Chang, T.-J., Chen, L.-C., Chen, M.-H., et al. (2010). Therapeutic efficacy and microSPECT/CT imaging of 188Re-DXR-liposome in a C26 murine colon carcinoma solid tumor model. *Nuclear Medicine and Biology*, 37, 95–104.
 53. Li, S., Goins, B., Zhang, L., & Bao, A. (2012). Novel multifunctional theranostic liposome drug delivery system: Construction, characterization, and multimodality MR, near-infrared fluorescent, and nuclear imaging. *Bioconjugate Chemistry*, 23, 1322–1332.
 54. Lee, H., Shields, A. F., Siegel, B. A., Miller, K. D., Krop, I., Ma, C. X., et al. (2017). (64)Cu-MM-302 positron emission tomography quantifies variability of enhanced permeability and retention of nanoparticles in relation to treatment response in patients with metastatic breast cancer. *Clinical Cancer Research*, 23, 4190–4202.
 55. Viglianti, B. L., Abraham, S. A., Michelich, C. R., Yarmolenko, P. S., MacFall, J. R., Bally, M. B., et al. (2004). In vivo monitoring of tissue pharmacokinetics of liposome/drug using MRI: Illustration of targeted delivery. *Magnetic Resonance in Medicine*, 51, 1153–1162.
 56. Lammers, T., Aime, S., Hennink, W. E., Storm, G., & Kiessling, F. (2011). Theranostic nanomedicine. *Accounts of Chemical Research*, 44, 1029–1038.
 57. Han, Z., McLaughlin, M. F., Woodward, J., Boll, R. A., Wall, J. S., Rondinone, A. J., et al. (2013). Gold coated lanthanide phosphate nanoparticles for targeted alpha generator radiotherapy. *PLoS One*, 8, e54531.
 58. Wang, S., Lin, J., Wang, Z., Zhou, Z., Bai, R., Lu, N., et al. (2017). Core-satellite polydopamine-gadolinium-metallofullerene nanotheranostics for multimodal imaging guided combination cancer therapy. *Advanced Materials*, 29.
 59. McDevitt, M., McDevitt, M., Alessandro, R., Carlos, H. V., Jason, P. H., Shanna, R. S., et al. (2010). Imaging and treating tumor vasculature with targeted radiolabeled carbon nanotubes. *International Journal of Nanomedicine*, 5, 783.
 60. Avila-Rodriguez, M. A., Selwyn, R. G., Hampel, J. A., Thomadsen, B. R., DeJesus, O. T., Converse, A. K., et al. (2007). Positron-emitting resin microspheres as surrogates of 90Y SIR-spheres: A radiolabeling and stability study. *Nuclear Medicine and Biology*, 34, 585–590.
 61. Zhou, M., Melancon, M., Stafford, R. J., Li, J., Nick, A. M., Tian, M., et al. (2016). Precision nanomedicine using dual PET and MR temperature imaging-guided photothermal therapy. *Journal of Nuclear Medicine*, 57, 1778–1783.
 62. Cui, L., Xiong, C., Zhou, M., Shi, S., Chow, D. S. L., & Li, C. (2018). Integrin $\alpha\beta3$ -targeted [64Cu]CuS nanoparticles for PET/CT imaging and photothermal ablation therapy. *Bioconjugate Chemistry*, 29, 4062–4071.
 63. Zhou, M., Song, S., Zhao, J., Tian, M., & Li, C. (2015). Theranostic CuS nanoparticles targeting folate receptors for PET image-guided photothermal therapy. *Journal of Materials Chemistry B*, 3, 8939–8948.
 64. Liu, Q., Qian, Y., Li, P., Zhang, S., Wang, Z., Liu, J., et al. (2018). The combined therapeutic effects of 131 iodine-labeled multifunctional copper sulfide-loaded microspheres in treating breast cancer. *Acta Pharmaceutica Sinica B*, 8, 371–380.
 65. Yang, W., Guo, W., Le, W., Lv, G., Zhang, F., Shi, L., et al. (2016). Albumin-bioinspired Gd:CuS Nanotheranostic agent for in vivo photoacoustic/magnetic resonance imaging-guided tumor-targeted photothermal therapy. *ACS Nano*, 10, 10245–10257.
 66. Li, B., Tang, J., Chen, W., Hao, G., Kurniawan, N., Gu, Z., et al. (2018). Novel theranostic nanoplatform for complete mice tumor elimination via MR imaging-guided acid-enhanced photothermo-/chemo-therapy. *Biomaterials*, 177, 40–51.
 67. Fan, Q., Cheng, K., Hu, X., Ma, X., Zhang, R., Yang, M., et al. (2014). Transferring biomarker into molecular probe: Melanin nanoparticle as a naturally active platform for multimodality imaging. *Journal of the American Chemical Society*, 136, 15185–15194.
 68. Zhang, R., Fan, Q., Yang, M., Cheng, K., Lu, X., Zhang, L., et al. (2015). Engineering melanin nanoparticles as an efficient drug-delivery system for imaging-guided chemotherapy. *Advanced Materials*, 27, 5063–5069.
 69. Yang, X., Hong, H., Grailer, J. J., Rowland, I. J., Javadi, A., Hurley, S. A., et al. (2011). cRGD-functionalized, DOX-conjugated, and 64Cu-labeled superparamagnetic iron oxide nanoparticles for targeted anticancer drug delivery and PET/MR imaging. *Biomaterials*, 32, 4151–4160.
 70. Feng, L., Cheng, L., Dong, Z., Tao, D., Barnhart, T. E., Cai, W., et al. (2017). Theranostic liposomes with hypoxia-activated pro-drug to effectively destruct hypoxic tumors post-photodynamic therapy. *ACS Nano*, 11, 927–937.
 71. Xue, X., Huang, Y., Bo, R., Jia, B., Wu, H., Yuan, Y., et al. (2018). Trojan Horse nanotheranostics with dual transformability and multifunctionality for highly effective cancer treatment. *Nature Communications*, 9, 3653.
 72. Yu, B., Goel, S., Ni, D., Ellison, P. A., Siamof, C. M., Jiang, D., et al. (2018). Reassembly of 89Zr-labeled cancer cell membranes into multicompartmembrane-derived liposomes for PET-Trackable tumor-targeted theranostics. *Advanced Materials*, 30, e1704934.